TECHNISCHE
UNIVERSITÄT
WIEN

DIPLOMARBEIT

Characterisation of cell membrane lipids of the thermophilic archaeon Sulfolobus acidocaldarius using high-performance thin layer chromatography and mass spectrometry

AUSGEFÜHRT AM INSTITUT FÜR
CHEMISCHE TECHNOLOGIEN UND ANALYTIK
DER TECHNISCHEN UNIVERSITÄT WIEN

UNTER DER ANLEITUNG VON
UNIV.PROF.MAG.DR. MARTINA MARCHETTI-DESCHMANN
UND
AO.UNIV.PROF.MAG.DR. ERNST PITTENAUER ERNST

DURCH
PETER SANDBICHLER

10.03.2020

Peter Sandbichler

Abstract

Cell membrane lipids of archaea differ significantly in their chemical structure from typical eubacterial cell membrane lipids, instead of glycerol ester-bond lipids archaea exclusively form glycerol ether-bond lipids. The lipid part itself is formed by connecting isoprene building blocks up to a C20-back bone (i.e. phytanol) exhibiting multiple methyl branchings. The membranes mainly consist of diphythanyl glycerol- and dimeric bis-diphythanyl glycerol-based lipids differing in their polar head groups (e. g. phosphoinositol, dihexoside etc.). Structural variation in the bis-diphythanyl glycerol-based lipid portion strongly depends on the growth conditions of *Sulfolobus acidocaldarius* as e.g. cyclopentane-ring formation. Archaeal lipids were analyzed by high-performance thin layer chromatography (normal phase as well as reverse-phase). For practical reasons, normal phase HPTLC was used. As lipid staining agent primuline was used being fully compatible with subsequent mass spectrometric analysis. This analytical strategy was applied to archaeal lipid extracts dissolved in different extraction solvents (methanol/chloroform, isopropanol/dimethylsulfoxide). After TLC separation the separated lipids were scraped from the TLC plate, extracted from the stationary phase and measured by mass spectrometry. Final mass spectrometric detection was performed by matrix-assisted laser desorption/ionization in combination with either a reflectron time-of-flight or a hybrid quadrupole/ reflectron time-of-flight. After optimizing measurement conditions for the samples like adapting the matrix system, laser power and rastering over the sample during the desorption/ionization process the different lipids were analyzed. During this thesis an algorithm was developed that allows to deduce the number of cyclic structures from isotopic structures detected in the different samples.

Data on the detailed composition of archaeal lipids will serve as valuable information for subsequent liposome experiments for drug incorporation.

Contents

1 Introduction

1.1 Aim of the study

Nowadays, many drugs have to be administered to patients via injections, which is particularly unpleasant for patients on long-term medication and makes therapy more difficult.
The aim of our collaborator is to provide delivery systems allowing to administer many of these drugs (cancer therapeutics, insulin, etc.) in the form of tablets. For this purpose, the active ingredients are coated with special lipids and thus protected in the stomach against digestive enzymes and gastric acid. They remain in the intestine long enough to effectively transfer the active ingredient to the organism. The lipids used for this protective sphere, which is also called liposome, are harvested from biotechnological processes involving specialized bacteria, and have to be investigated in detail. They originate from the cell membrane of archaeon *S. acidocaldarius*, the lipid extracts of which are provided by our collaborator. The aim of this study is the identification of the membrane components and detailed characterization of these lipids. For this a reproducible high-performance thin layer chromatography (HPTLC) method was developed. Furthermore, lipid samples from different production processes were measured by matrix-assisted laser desorption ionisation (MALDI) time-of-flight (TOF) mass spectrometry (MS) and compared to each other. Additionally, an estimation about necessary quantification abilities in order to make such comparisons has been made.

1.2 Sulfulobus acidocaldarius

In 1972, T.D. Brock reported the isolation and characterization of a new genus of sulfur-oxidizing bacteria. Due to its peculiarities he called the organism *Sulfolobus acidocaldarius* which indicates its preferred habitat, a hot acidic environment [1]. Nowadays, we know that life forms like Sulfolobus belong neither to the eukaryotes nor the bacteria, but form their own domain, the archaeae. Although both bacteria and archaeae are prokariotes, they differ strongly in several aspects. An essential difference between the two life forms lies in the composition of their cell membrane. The cell membrane lipids of bacteria consist of two fatty acid residues which are bound to the hydroxy group of a glycerol molecule via an ester bond. In archaeae, isoprenoid chains take the place of fatty acids and are linked to glycerol 1-phosphate backbones via an ether bond, as shown in figure 1, forming so called diether lipids (DEL).

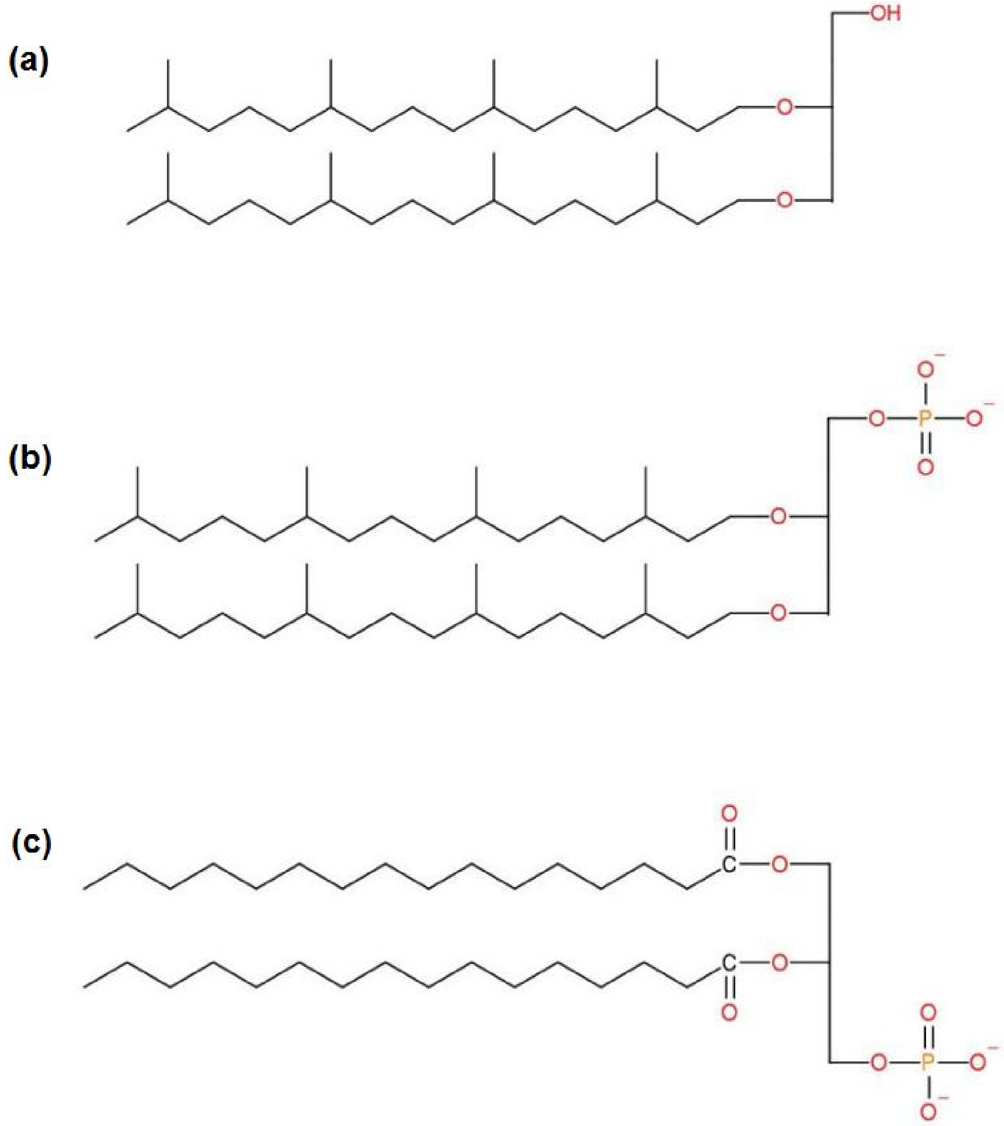

Figure 1: Schematic structure of (a) a DEL with diphytanyl glycerol diether (DGD) as an example, (b) IP-DGD, one of the typical cell membrane lipids of *S. acidocaldarius*, (c) a typical bacterial cell membrane phospholipid.

Another property of the phylum crenarchaeota is that in addition to the DEL, membrane spanning bipolar tetraether lipids (TELs) are formed by condensation of two diether lipids. A TEL that occurs in the membrane of *S. acidocaldarius* is glycerol-dialkyl-glycerol-tetraether (GDGT), whose schematic structure is shown in figure 2. TELs form a membrane monolayer, making it almost impossible for ions and protons to penetrate this barrier. For this reason, Crenarchaeae like *S. acidocaldarius* are very stable at low pH values and high temperatures [2],[3].

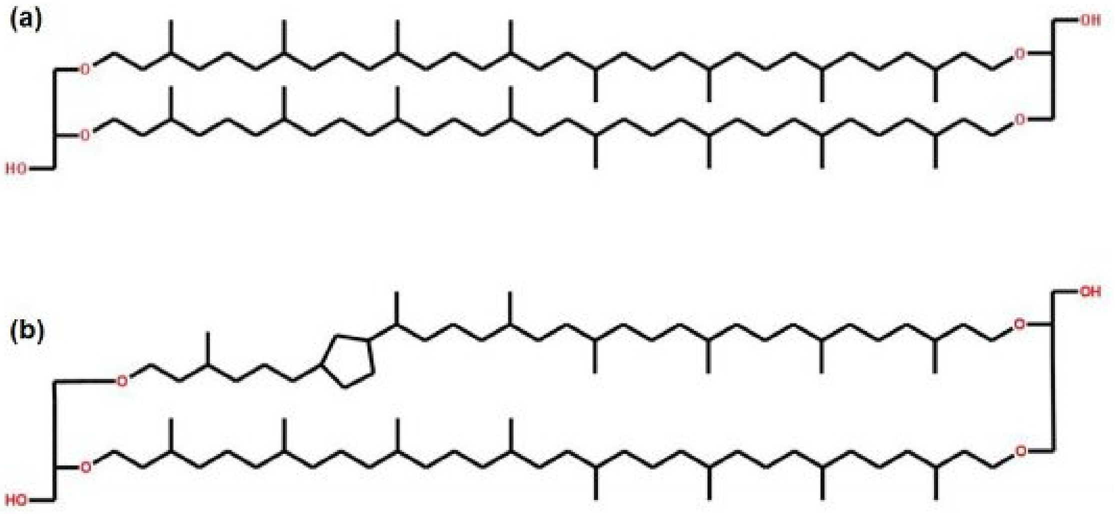

Figure 2: Schematic structure of (a) GDGT 80;0 and (b) GDGT 80;1.

TELs also form so called cyclopentane rings in their isoprenoid core structures as adaptation to e.g. higher temperatures, as shown in figure 2b. The number of rings formed is influenced by the prevailing environmental conditions and upto 8 rings can be formed in a TEL [4]. To describe these lipids, the number of carbon atoms in the isoprenoid chains and the number of cyclopentane in these chains are given after the names, e.g. GDGT 80;1 means that the isoprenoid chains consist of a total of 80 carbon atoms and one cyclopentane is present in the structure. By the formation of one cyclopentane ring, the lipid loses two hydrogen atoms.

1.3 Thin-Layer Chromatography

Thin layer chromatography (TLC) is a very simple and fast method to separate molecules based on their polar or apolar characteristics. The principle of separation is based on a stationary and a mobile phase and the interaction of the molecules under investigation with these. A distinction is made between normal phase and reversed phase TLC. In case of normal phase TLC (NP-TLC), the stationary phase has polar properties and the mobile phase has apolar properties. The stationary phase consists of a fine-grained material such as silica gel which is deposited on a carrier such as aluminum. In the case of silica gel, this material consists of a three-dimensional lattice with alternating silicon and oxygen atoms, with OH groups on the surface. These interact with the polar components of the molecules in the sample to be analyzed. Table 1 shows different stationary phases and their respective applications. Other examples for stationary phases are aluminum oxide used for steroids and terpenes.

Table 1: Stationary phases used in TLC Analysis, adapted from [5]

Stationary phase	Principle	Applications
Cellulose ion exchangers	Anion exchange	Amino acids, peptides
Polyamide	Partition chromatography	Phenolic natural substances
Silica Gel	NP chromatography	Most frequent application
RP-2, RP-8, RP-18	RP chromatography	Lipids, aromatics
Kieselguhr	RP separations	Aflatoxins, herbicides

To apply a sample to the TLC plate, it has to be in solution. The choice of solvent depends on the substance to be analyzed. The solvent must be able to dissolve the analyte well and have a certain volatility to evaporate on the TLC plate. Most lipids in general are apolar compounds that are dissolved in apolar solvents like pentane or cyclohexane. However, there are some lipids that are better soluble in apolar solvents due to their apolar characteristics. Since the membrane lipids of *S. acidocaldarius* are analyzed, which include phospholipids that have both an apolar and a polar part, polar solvents with high volatility such as methanol or chloroform are used. Also dimethylsulfoxide (DMSO) and isopropanol are very potent polar solvent that can be used to dissolve polar lipids. The only problem with DMSO is the very high evaporation temperature, which severely limits the use of the solvent for mass spectrometry. TLC plates can only be developed when the application solvent has evaporated completely. Before the developing of the TLC plate, the sample is applied to the lower end of the plate via a glass capillary.

The height of the sample spots is marked on the plate's edge. After the solvent, in which the sample was dissolved, has evaporated from the TLC plate, the plate is placed in a development chamber containing the mobile phase, whereby the bottom of the chamber should only be slightly covered with the mobile phase. The applied sample spot must not touch the mobile phase. The mobile phase moves to the top of the TLC plate by capillary forces and moves the sample upwards because the mobile phase is always chosen in a way that the sample is soluble in it.

The very polar OH groups on the surface of the silica gel counteract this upward force and slow down the molecules of the sample depending on their polarity. The more polar a molecule, the slower it moves upwards in the TLC plate. Just before the mobile phase reaches the top of the TLC plate, the plate is removed from the developing chamber, the front of the mobile phase is marked and the plate is dried. Figure 3 shows a developed TLC plate. In most cases, the separated spots are not visible on the dried TLC plate and therefore have to be stained. The analytes investigated are lipids, to make them visible there are several staining methods. Among others, coomassie brilliant blue staining is widely used to stain phospholipids. However, to analyze lipids after TLC separation by MS, staining compatible with MS is required. Visiualization by primuline is fully compatible with subsequent MALDI-MS analysis. A 0.05% primuline solution can be used making lipids visible under UV light of 365 nm wavelength.

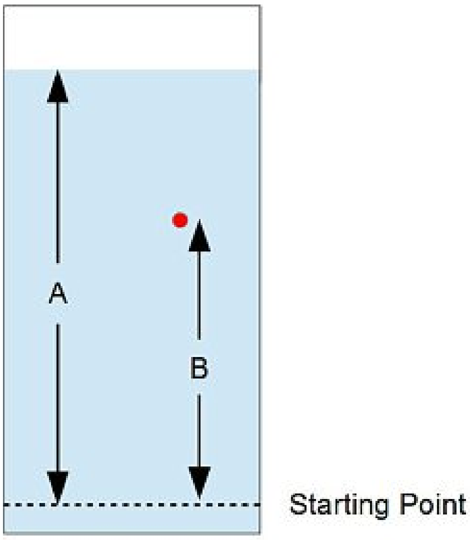

Figure 3: A developed TLC plate, where the upper edge of the blue colored area represents the travel distance of the solvent front and the red circle indicates the upwards traveled analyte.

To characterize the separation the retention factor R_f value

$$R_f = B/A \tag{1}$$

is calculated for each spot which simply represents the ratio of the traveldistance B of a spot to the traveldistance A of the front of the mobile phase [6].

A distinction is generally made between TLC chromatography and HPTLC, with the largest differences being in the particle and pore size of the sorbents, where 5 µm is suitable for HPTLC. The thickness of the sorbents is 200 µm for HPTLC plates and 250 µm for TLC. HPTLC plates are generally smaller than TLC plates because the separation of analytes occurs over smaller distances. Advantages of HPTLC over TLC are shorter development times, which is related to the shorter path length of the development, higher efficiency and better quantification capabilities. An automatic sprayer is usually preferred over manual spotting of the sample onto the TLC plate.

1.4 Mass spectrometry

Mass spectrometry is a highly developed technique of analysis and is used in almost every field of natural science. Many types of substances can be analyzed with extremely high sensitivity, information can be obtained even if the analyte is only present in the attomolar range. In addition to the chemical composition of a sample the structure of the individual molecules can be determined and their quantity can be measured, at least in a relative quantitative manner. Therefore the field of application of mass spectrometry is enormously large and extends far beyond scientific research, reaching from doping control in sports to climate research and isotope ratio determination in archaeology.

1.4.1 Principle

A mass spectrometer is used to measure the mass-to-charge ratio (m/z) of an ionized molecule. As a first step, the analytes are transferred into the gas phase and ionized. Depending on the ionization technique, this process takes place under high vacuum or at intermediate/atmospheric pressure. An electric field accelerates the ions towards the analyzer which separates them according to their m/z value. A detector then registers the ions and displays the measured values in a mass spectrum [7]. Figure 4 shows the principle schematically.

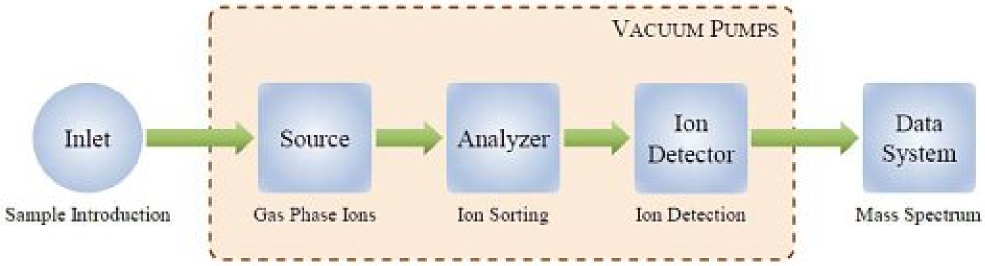

Figure 4: Principle of a mass spectrometer, adapted from [8]

1.4.2 Ionization techniques

In order to be able to examine analytes, they must first be ionized. This process can happen in the liquid phase as well as in the solid state, under atmospheric pressure or high vacuum. A distinction is made between soft and hard ionization methods. The choice of ionization method has a decisive influence on the spectrum. While hard ionization methods are characterized by strong fragmentation, they provide a strong ion yield compared to soft ionization methods. The choice of ionization method must therefore be adapted to the analytes. Both the specific physicochemical properties and the internal energy transferred to the analytes during ionization have to be taken into account. The desired measurement result must be considered as well, as it heavily depends on the ionization technique. In order to study analytes present in low concentration and to obtain a spectrum characterized by low fragmentation, MALDI was used as ionization technique in this work.

- Ionization techniques operating at atmospheric pressure
  - Electrospray ionization (ESI)
  - Desorption electrospray ionization (DESI)
  - Atmospheric-pressure chemical ionization (APCI)
  - Atmospheric pressure laser ionization (APLI)
  - Low temperature plasma (LTP)
  - Direct analysis in real time (DART)
- Ionization techniques operating under high vacuum.
  - Electron impact ionization (EI)
  - Chemical Ionization (CI)
  - Matrix-assisted laser desorption/ionization (MALDI)
  - Fast Atom Bombardment (FAB)
  - Field Desorption (FD)
  - Field Ionization (FI)
  - Photoionization (PI)

1.4.2.1 Matrix-assisted laser desorption/ionization

In bioanalytics it is especially important to have a reliable ionization method at hand where molecules with several thousand Daltons (Da) can be ionized without losing a large portion of the signal to fragmentation. MALDI is one of the so called soft ionization methods, imparting little residual energy to the analyte and thus reducing signal losses due to fragmentation.

The analyte is mixed with a matrix dissolved in an organic solvent such as acetonitrile or MeOH. Matrices show a strong absorption in the UV or IR range and can thus be used to ionize the analyte when exposed to laser light. MALDI is a further development of laser desorption/ionization, utilizing pulsed high-energy photons from UV or IR lasers, leading to desorption and ionization of an analyte.

With the development of a method in which an analyte is connected to a UV-absorbing matrix by co-crystallization, Franz Hillenkamp and Michael Karas were able to establish MALDI as one of the most important techniques in bioanalytics. The researchers discovered that in a mixture of two substances, one of which absorbed the laser light very well and the other one absorbing it poorly, both components were ionized at the energy density of a laser pulse, which in the unmixed state would have had an ionizing effect only on the highly absorbing component [9].

In the case of MALDI, matrices form the highly absorptive component, the analyte forming the low absorbtive one. A mixture of analyte and matrix is prepared, with the matrix in high excess. By pulsed laser radiation the analyte can thus be ionized and brought into the gas phase.[6].

The matrix absorbs the laser radiation and simultaneously protects the analyte from fragmentation. Afterwards, it transfers the absorbed energy to the analyte which is necessary for desorption and ionization, schematically shown in 5. The matrix molecules are involved in proton interactions with the analytes whereby the matrix can act both as donor and acceptor. During this process, hydrogen or alkali ions are attached to the analytes. Ions generated by the abstraction of a proton $[\mathrm{M\text{-}H}]^-$ or by the absorption of a proton $[\mathrm{M+H}]^+$ or by the addition of a cation $[\mathrm{M+Cat}]^+$ in this process are called *ions of the molecular species.* [7]. Table 2 shows common MALDI matrices.

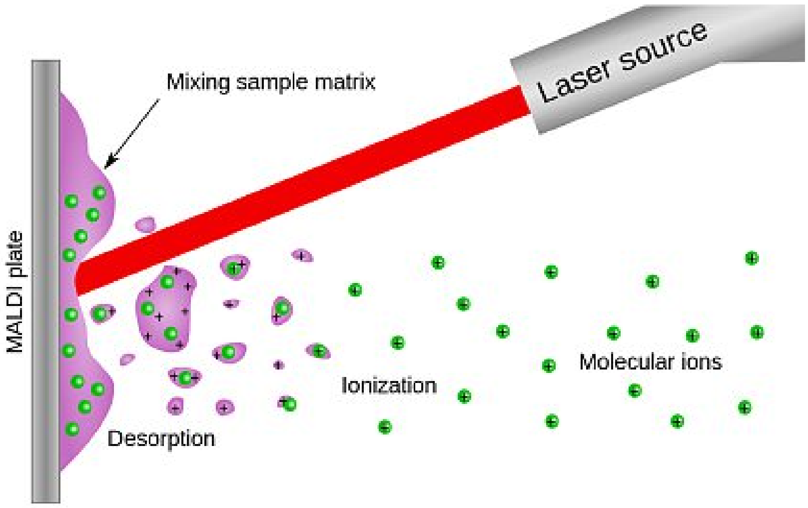

Figure 5: Principle of ionization and desorbtion process in MALDI, adapted from [10].

Table 2

Matrix	Abbreviation	Analyte
2,5-Dihydroxybenzoic acid	DHB	Peptides, proteins, organic molecules
9-Aminoacridine	9-AA	Lipids
α-Cyano-4-hydroxycinnamic acid	CHCA	Carbohydrates, peptides, proteins
Dithranol	DIT	Lipids, synthetic polymers
Trans-3-indoleacrylic acid	IAA	Synthetic polymers
Trihydroxyacteophenone	THAP	Lipids, carbohydrates, oligonucleotides

1.4.3 Mass analyzers

After successful ionization of the analyte molecules, the goal of mass spectrometry is to determine as accurately as possible the m/z value of these components which is determined by the use of electric and/or magnetic fields. For this measurement process, the interference-free interaction of the analyte ions with these fields is of utter importance which is why a high vacuum is required in the mass analyzers. Any collision interaction of an analyte ion falsifies the calculation of the m/z value and leads to mass resolution for the recorded spectra.

1.4.3.1 Time-of-Flight mass spectrometry

As the name suggests, a TOF analyzer measures the flight time of an ion in a field-free region inside a hollow tube. After their ionization, the ions gain potential energy E_{pot} by passing through an electrical potential V_s according to

$$E_{pot} = qV_s \quad , \tag{2}$$

where

$$q = ze \tag{3}$$

is the charge of the ion, with e being the elementary charge and z the number of charges in the ionized analyte. The potential applied is usually 20kV.

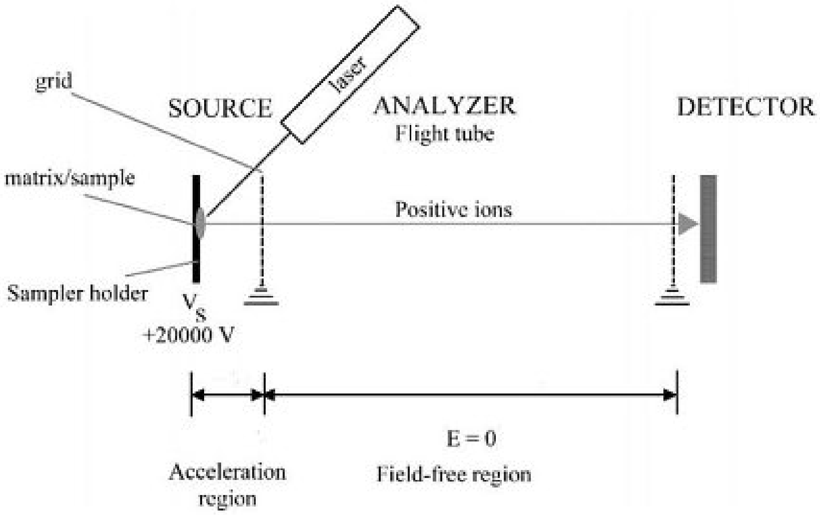

Figure 6: TOF schematically shown for a positive ion analysis. The potential difference is applied between grid and sample holder and accelerates the ion direction of the analyzer. Adapted from [7]

By this energy gain the ions are accelerated and, by equating the potential with the kinetic energy

$$E_{kin} = \frac{1}{2}mv^2 = ezV_a = E_{pot} \quad , \tag{4}$$

in which m represents the mass and v the velocity, the flight time of the ion can be calculated by transforming (4) and substituting v with s/t. Therefore, the equation

$$t = \frac{s}{\sqrt{\frac{2\,ezV_a}{m}}} \tag{5}$$

can be obtained where s is the field-free distance between ion source and detector. The flight time squared is thus directly proportional to the m/z value

$$\frac{m}{z} = At^2 \tag{6}$$

where $A = \frac{2eV_a}{L^2}$ summarizes the constant parameters of the instrument.
This equation also shows, why a mass spectrometer cannot measure the mass of an ion directly, as it can not distinguish between an ion of mass $\mathrm{m_1}$ with a charge of $\mathrm{z_1}$ and an ion with mass $\mathrm{m_2} = 2\mathrm{m_1}$ and charge $\mathrm{z_2} = 2\mathrm{z_1}$. The principle of this process is shown in figure 6. To obtain the resolution of the TOF in a first approximation, the first derivative of (6) can be calculated:

$$\frac{1}{z}dm = A\,2t\,dt \quad . \tag{7}$$

Inserting for z and reshaping the equation results in the relation

$$\frac{m}{dm} = \frac{t}{2dt} \quad . \tag{8}$$

The mass resolution is therefore given by

$$R = \frac{m}{\Delta m} = \frac{t}{2\Delta t} \approx \frac{L}{2\Delta x} \quad , \tag{9}$$

where Δx is the spatial extent of the ion package that approaches the detector, Δm and Δt are the full width at half maximum (FWHM) values on their respective scale.
This equation shows that the greater the field-free flight path in the mass spectrometer, the better the resolution. However, for a long flight tube, a loss of signal intensity must be taken into account, since the ion beam encloses a finitely large solid angle and collisions with residual gas molecules

occur despite the high vacuum. The resolution can be further improved by a reflectron TOF or by delayed pulsed extraction [7].

Delayed Pulsed Extraction

During the ionization process, not all identical ions obtain the exact same kinetic energy, they are subject to a certain distribution. The direction of the momentum vector also differs, therefore the velocity component in the direction of the analyzer also varies. To counteract this problem, a short time frame is inserted between ionization and extraction from the ion source when using delayed pulsed extraction. During this time, the ions move into a field-free region. Those with a high velocity fraction in the direction of the analyzer move further away from the sample holder than those with less velocity in this direction.

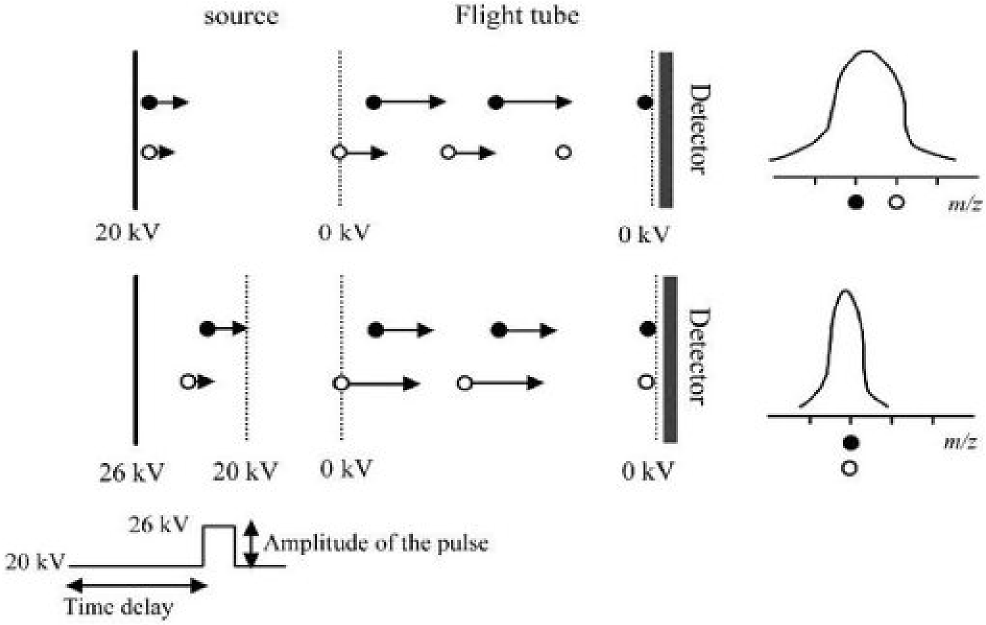

Figure 7: Continuous (top) vs. delayed pulsed (bottom) extraction of ions towards the field-free drift region on a TOF analyzer schematically, adapted form [7]

After a certain time, an electric pulse accelerates the ions towards the detector, its strength depending on the ions' location. This pulse transfers more energy to the ions having originally received less momentum towards the detector and less to those having already advanced further towards the detector, thus correcting the energy differences for ions of the same m/z value and improving resolution. The processes are shown in figure 7.

By adjusting the time frame between ionization and extraction and the voltage of the pulse, ions can be focused specifically on the detector. However, it should be noted that these parameters are mass-dependent, a perfectly focused device for lighter ions will show poorer resolution for ions of greater mass. Therefore, delayed pulsed extraction will only provide satisfactory resolution improvements for a part of the mass spectrum [7].

Reflectron

Furthermore, the resolution can be improved by using a reflectron. A reflectron usually consists of a series of grating electrodes, which form an electrical potential

$$V_R = DE \quad , \tag{10}$$

where D is the length of the reflectron and E the electrical field inside the reflectron, shown in figure 8. It is positioned behind the field-free region where the detector is usually located. An ion with kinetic energy E_{kin} penetrating the reflectron with a speed v_i enters the reflectron to a depth d:

$$d = \frac{E_{kin}}{eE} = \frac{eV_a}{eV_R/D} = \frac{V_a D}{V_R} \quad . \tag{11}$$

v_i represents only the part of the ion's velocity vector which is parallel to the direction of the potential of the reflectron. At the point d, the velocity of the ion in gradient direction of the reflectron is zero and its average velocity is $v_i/2$. Therefore, the time to reach the point d is equal to

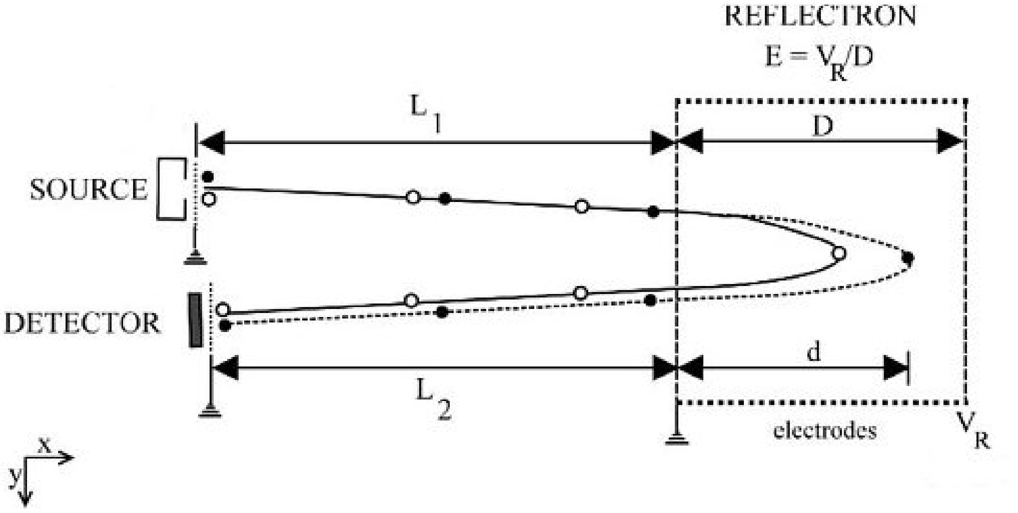

Figure 8: RTOF schematically, adapted from [7]

$$t_0 = \frac{2d}{v_i} \quad . \tag{12}$$

The ion's velocity component perpendicular to the potential gradient does not interact with the reflectron potential and remains unchanged. This is important because the detector is mounted slightly next to the ion source and can be hit by the reflected ion beam. Ions with higher kinetic energy penetrate deeper into the potential of the reflectron than the ones with lower energy. Ions with higher energy spend more time

$$t_r = \frac{2d}{v_i/2} = \frac{4d}{v_i} \tag{13}$$

in the reflectron. When leaving the reflectron potential, the ions have the same velocity v_i as when entering but move in opposite directions. The ion has a total flight time of

$$t = \frac{L_1 + L_2 + 4d}{v_i} \quad , \tag{14}$$

with L_1 being the distance between ion source and reflectron and L_2 being the distance between reflectron and detector. This procedure allows to compensate for the ions' initial differences in kinetic energy leading to an improved resolution of the spectrum [7].

1.4.3.2 Quadrupole

Quadrupole analyzers consist of four parallel rods, the axes of which are each attached to one corner of an imaginary square, as shown in figure 9. A radiofrequency alternating voltage $V cos(\omega t)$ is applied to these rods which is superimposed with a direct voltage U. Two opposite rods are connected to the same pole each. This creates an electric field which in practice oscillates at about 1MHz.

Assuming the cross section of the bars represents the x-y plane, ions drift in z direction into the quadrupole and are accelerated in the direction of a bar of opposite charge. Due to the alternating polarity of the voltage the ions oscillate along the z plane. The mass selection results from the superposition of DC and AC voltage. The oscillation paths are only stable for ions with the appropriate m/z value, the remaining ions colliding with the rods. The width of this m/z value is defined by the ratio 2U/V. In comparison to TOF analyzers, the mass separation in the quadrupole is not dependent on the kinetic energy of the ion. However, it has to be considered that if the kinetic energy is too high, ions cannot be influenced by the quadrupole field because the interaction time is too short and all ions can pass through. If the kinetic energy is too low, the quadrupole switches to the next m/z value, whereby the ions are no longer in resonance with the field and are lost.

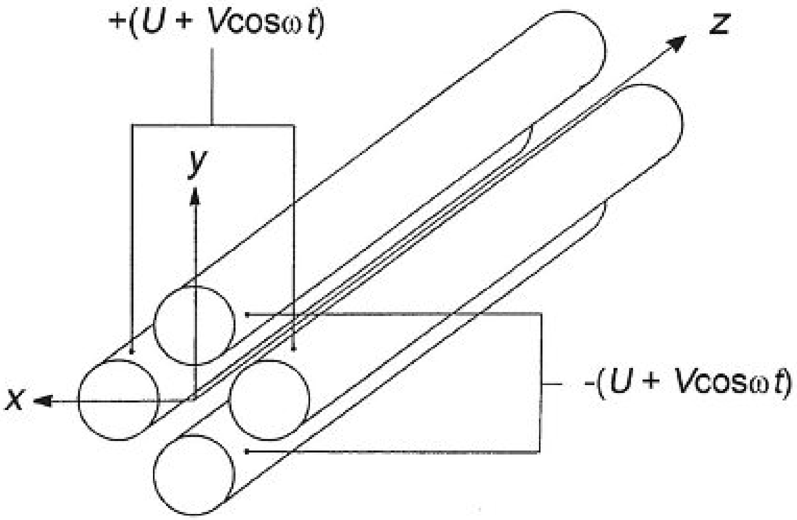

Figure 9: Schematic structure of a quadrupole with round rods, adapted from [11]

1.4.3.3 Fourier transform ion cyclotron resonance

When charged particles enter a magnetic field, they are subjected to the effect of the Lorentz force which is proportional to the strength of the magnetic field B, their charge q and their velocity component v which is perpendicular to the magnetic field B. In a cyclotron, the Lorentz force acts as a centripetal force

$$F_{cp} = qvB \tag{15}$$

and opposes the centrifugal force

$$F_{cf} = \frac{mv^2}{r} \tag{16}$$

forcing the ions to follow a circular trajectory of radius r. The cyclotron frequency ω_c is

$$\omega_c = 2\pi\nu = \frac{v}{r} = \frac{qB}{m} \tag{17}$$

and accordingly dependent on the strength of the magnetic field, the mass and the charge of the ion but not dependent on the velocity of the ion. Ions with a radius greater than that of the cell are lost. Superconducting magnets are used to generate magnetic fields of the required strength between 7 and 15 T. To obtain the m/z value, the cyclotron frequency must be determined.

Therefore, all ions are simultaneously excited by a high frequency scan resulting in a trajectory of the ions near the wall of the ICR cell. The detected complex wave can be transformed from time space to frequency space by a Fourier transformation. Ions which are excited with the same energy, and therefore the same potential V_c, by an AC frequency in the same time period T, have the same radius

$$r = \frac{V_c T}{B} \quad , \tag{18}$$

giving them a trajectory near the detection plates in the wall. The radius is independent of the ions' m/z value but the frequency of the ions differs. The better the vacuum and the longer the observation time, the better the resolution. The calculation, mostly done with SWIFT (Stored waveform inverse Fourier transform), is very complex, because the sampling velocity has to be at least twice as high as the highest frequency according to the Nyquist theorem.

1.4.4 Microchannel plate detectors

After passing the mass analyzer, the ions are converted into an electrical signal at the detector. Therefore, the ions are strongly accelerated towards a conversion dynode which is kept at a strong potential between ± 3kV and ± 30kV. When an ion hits this dynode, secondary particles are emitted from it. Through an avalanche-like effect, these electrons are multiplied inside the electron multiplier and create a current proportional to the number of ions hitting the conversion dynode, an amplification of the factor 10^6 can be achieved. In contrast, the so-called micro channel plates are based on a similar principle, shown in figure 10. They have a very low response time and are therefore preferred in mass spectrometry. Microchannel plates consist of

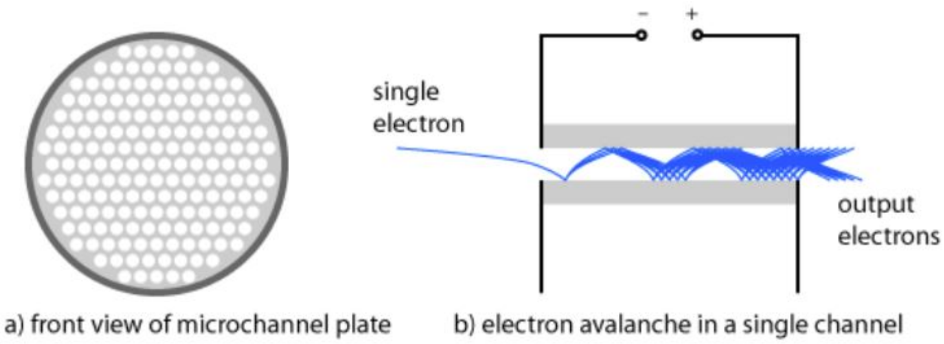

Figure 10: Schematic illustration of a micro channel plate in front and side view. [12]

a slab of highly resistive material like glass with many channels in it and are slightly tilted which ensures that incoming ions hit the walls of the channels. By connecting several multi channel plates in series, a multiplication of up to a factor 10^8 can be realized. Since the channels are only a few millimeters long the response time is very low. A single anode is attached to the outlet and registers all electrons exiting the channels. The current can be measured and the ion intensity can be calculated.[7]

1.5 Tandem Mass Spectrometry

In order to obtain information about the structure of a material, ions can be fragmented into their constituent parts using tandem mass spectrometry. The selection of the precursor ion can be done *in-space* or *in-time*. By coupling two mass analyzers, the ionization, precursor ion selection, collision-induced dissociation (CID) of the precursor ions and mass analysis of the fragments occur in different regions of the instrument, hence it is called tandem MS in-space. For tandem-in-time instruments, all these processes happen in the same region of the instrument and only one mass analyzer is needed.

In this master thesis, in-space instruments were used, which is why they will be explained in more detail. If two mass analyzers are coupled, the first selects a precursor ion, an ion with a specific m/z value to be fragmented, from the sample. This precursor ion is then fragmented in a collision cell which is usually done by collision with an inert gas such as argon supplying the precursor ion with energy. Part of the impact energy is absorbed by the precursor ion as internal energy resulting in bond breaks and fragmentation of the ion into smaller ions which are often easier to identify. This technique is called collision-induced dissociation (CID). In most cases, these product ions are more clearly identifiable than the precursor ion which makes it possible to infer its identity. The fragments are then separated by the second mass analyzer according to their m/z value.

Another method of fragment investigation is post source decay (PSD). In this procedure the ions produced by MALDI already contain enough energy after ionization and decay into fragments on their trajectory. With linear TOF, these product ions can not be distinguished from their precursor ions, since they arrive at the detector at the same time. However, if they pass through a reflectron, their flight time differs due to their lower kinetic energy and the fragments can be distinguished. Fragments with lower kinetic energy do not penetrate the reflectron as deeply as fragments of higher kinetic energy. These differences in flight times can be used to calculate their respective m/z values.

1.6 Data Analysis

To evaluate the measurement result, the detected ions are displayed in a mass spectrum. The ions measured at the detector are plotted according to their abundance against their m/z ratio in a 2-dimensional plot, as shown in figure 11.

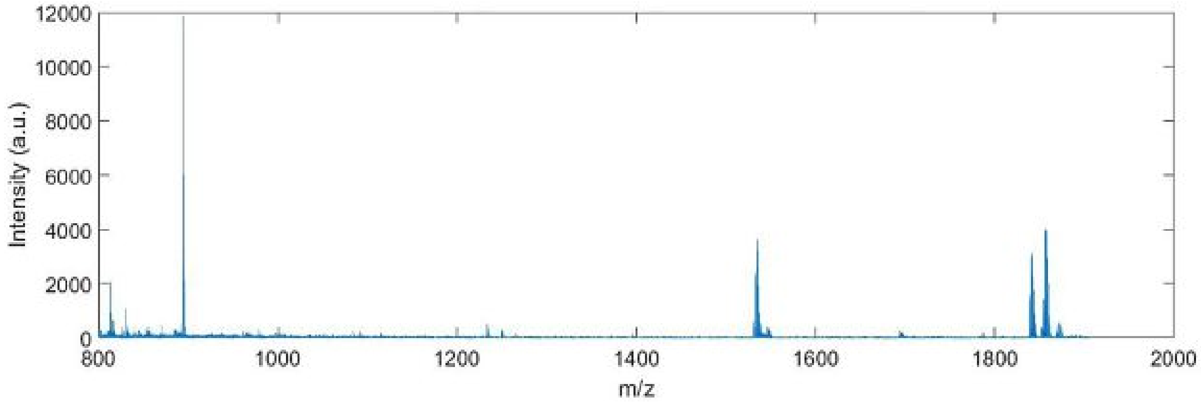

Figure 11: Mass spectrum of a sample analyzed in this thesis.

The scaling of the y axis does not correspond to the ions actually measured, but is represented in arbitrary units. The intensity of the different ions measured is compared. It should be noted that factors such as different ionization probabilities, fragmentation and, in the case of MALDI, a non-homogeneous distribution of the analyte on the target plate make quantification quite difficult and additional measures must be taken to improve this aspect.

1.6.1 Isotopes and isotopic distribution

Chemical elements occur with different numbers of neutrons in nature. If an atomic species has the same number of protons, but differs only in the number of neutrons, they are called isotopes. Isotopes have different mass numbers and are subject to a statistical distribution in nature. This distribution is also detected in mass spectra. The information obtained about the isotopic distribution by measurements with mass spectrometers can, for example, be used to determine the element composition or the number of charges of the measured ion. For small molecules, in most cases, the peak of the monoisotopic mass is the most abundant. The more atoms with stable isotopes a molecule contains, the more likely it is that one of these atoms is present in the form of a non primary isotope. This leads to the fact that for larger molecules the monoisotopic peak is no longer the most abundant one. The larger the number of measured ions, the more closely the measured distribution matches the theoretical distribution. To perform calculations based on the isotopic distribution, the instrument must be able to provide a true isotopic pattern, i.e. the measured spectrum must reflect the natural isotope distribution without too strong deviation.

1.6.2 Precision and accurate mass measurements

Mass precision is defined as the root-mean-square deviation for many repetitions of a measurement. The smaller this value is, the more precise the measurement is. Mass accuracy is the difference of the measurement and the actual mass of an ion. Mass precision and mass accuracy are of utmost importance for component identification measurements. The greater the mass of an ion, the more possibilities there are for its elemental composition. The more precise and accurate the measurement of this ion, the smaller the range of possible elemental compositions. To determine the mass of an ion as accurately as possible, accurate mass measurements are used. This involves measuring a sample with a known ion whose mass is as similar as possible to the ion under investigation. This ion is used for calibration. Subsequently, a sample with the ion to be investigated is measured. Due to the calibration with the known ion, systematic errors can be prevented very well, the mass of the unknown ion can be determined very precisely and the elemental composition can be determined more easily.

1.7 Instrumentation

1.7.1 Synapt G2 HDMS

Most measurements of the following experiments were performed on a MALDI Synapt G2 HDMS. Although the Synapt has two ion sources, only MALDI was used in this thesis. The instrument also has a quadrupole, a Triwave^{TM} section and an orthogonal acceleration RTOF (oa RTOF) analyzer. For ionization/desorption it uses a neodymium-doped yttrium-aluminum garnet (Nd:YAG) laser with a wavelength λ of 355nm. The laser's peak power is 25kW and it has a pulse energy of up to 50 µJ at 1 kHz repetition rate. A schematic illustration of the Synapt G2 HDMS is shown in figure 12.

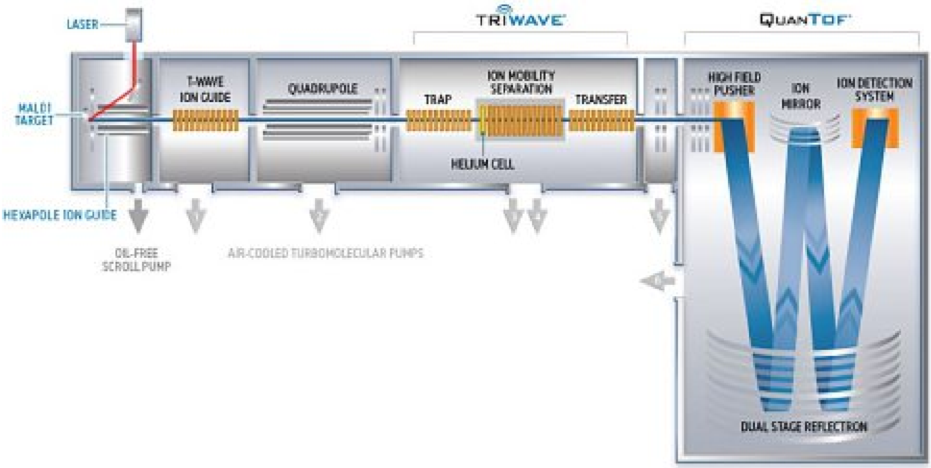

Figure 12: Schematic illustration of the Synapt G2 HDMS, adapted from [8].

The Synapt G2 HDMS has a intermediate pressure MALDI source. The quadrupole can be operated in different mass ranges, depending on the type of the RF-generator. In our case the 4 kDa mass range was chosen because of the low mass of our components. The quadrupole can be used in two different modes.

The first one is only applying an RF voltage to the quadrupole, whereby the quadrupole allows a high mass range of ions to pass through to the triwave section. To perform MS/MS experiments, the Synapt uses a quadrupole time-of-flight (qTOF) system. A quadrupole is coupled with a TOF. The quadrupole selects the precursor mass. Subsequently, the precursor ion is fragmented, in the case of the Synapt G2 HDMS this happens in the trap cell. The fragments pass through the triwave section without interacting with the ions. The m/z value of the fragments is then determined in the TOF. The second superimposes a resolving dc voltage, allowing a specific mass to be selected in the quadrupole for fragmentation experiments. After the ions have passed the quadrupole, they enter the triwave section of the device, shown in figure 13. This section consists of three T-Wave devices, all of them performing a certain task. The first T-Wave ion guide traps and accumulates the ions if ion mobility experiments are performed. In the second section, the IMS cell, the ions are separated according to their gas phase transport properties in electric fields in ion mobility experiments. In MS and MS/MS measurements the IMS cell has only a transfer function. The third element is the transfer cell. It works like the trap cell but has no gate to trap the ions. Ions can also be fragmented here. The collision energy in the trap and transfer cell can be up to 240 V each.

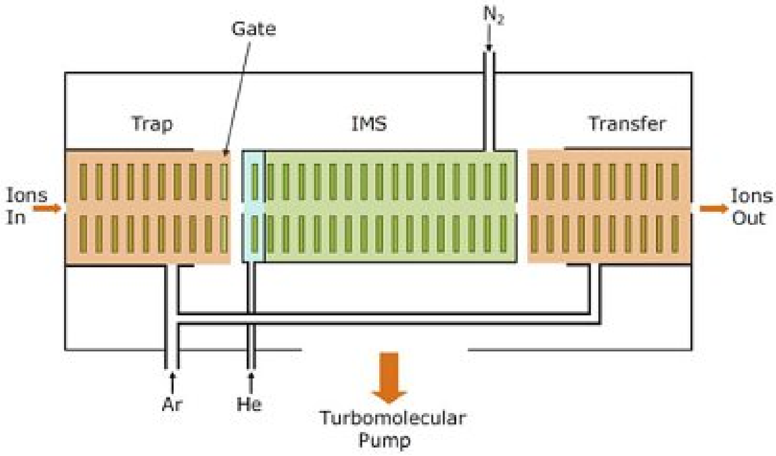

Figure 13: Schematic illustration of the triwave section, adapted from [8].

After passing the triwave section, the ions reach the oa-RTOF. In this RTOF, the ions are first accelerated orthogonally by a pulsed electric field. This orthogonal acceleration and the accelerating pulsed field improve the resolution of the mass spectrum because the RTOF analyzer calculates the mass based on the energy of the orthogonal pulsed electric field. Differences in kinetic energy in the ion beam coming from the ion source still lead to a slight deterioration in the resolution of the spectrum because the velocity component is still present, its influence however being greatly reduced. The measurement of the ions is done in duty cycles. Only after ions of a cycle have passed the oa-RTof and have been analyzed, the next charge of ions can be accelerated into the oa-RToF. Therefore, a certain part of the intensity is lost because not all ions from the ion source are accelerated into the mass analyzer. The Synapt G2 HDMS has a dualstage reflectron, shown in figure 14, which can be operated in reflectron mode and double reflectron mode.

For standard measurements (resolution up to 16000 FWHM[2]), the reflectron mode is used. For exact mass measurements and exact mass calibration, the W-mode is used (resolution up to 32000 FWHM[2]) which adds an additional ion mirror to increase the trajectory. Due to the reasons mentioned above, the W-mode is associated with higher losses in terms of sensitivity.

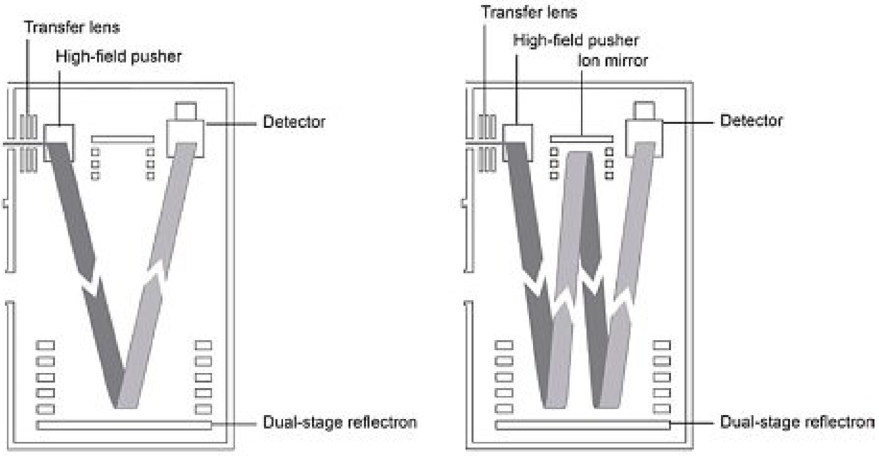

Figure 14: Schematic illustration of the dualstage reflectron, adapted from. [13]

1.7.2 Shimadzu MALDI-7090$^{\mathrm{TM}}$

Like the Synapt G2 HDMS, the Shimadzu Maldi-7090$^{\mathrm{TM}}$ has a Nd-YAG laser with 355nm wavelength and a maximum of 2kHz laser frequency. In comparison to the Synapt G2 HDMS, the Shimadzu MALDI-7090 has a high vacuum MALDI ion source. Fragmentation experiments are carried out by CID or by PSD. In our experiments the CID variant is used because the fragmentation energy of this method is higher than the PSDs'. The MALDI 7090 allows high energy CID up to 20 keV, which is used in lipid analyses to trigger charge remote fragmentation (CRF). This type of fragmentation provides important information about the presence and structure of isoprenoid chains. However, doing CID with a MALDI ion source, a laser power above threshold level is required, leading to a decrease in resolution for both precursor and product ions due to the concomitant velocity and spacial distribution of ions.To reduce axial spatial distributions, the Shimadzu MALDI-7090 incorporates a new technology called *Axial spatial distribution focusing* (ASDF). The so-called ASDF cell consists of two high transmission gratings to which a fast high voltage pulse can be applied. Similar to the delayed pulsed extraction, after the ions enter the ASDF cell, a high potential pulse is applied to the grid facing the ion source generating an E-field. This pulse bunching of the ions allows them to fly through the cell and correct the local distribution of the ions [14]. Thus, despite the curved field R-TOF without LIFT, resolutions of 10000 FWHM can be achieved [15] .

2 Materials and Methods

2.1 Chemicals

- Sigma-Aldrich, St. Louis, MO, USA:
  - Chloroform HPLC Plus, ≥99.9%, contains amylenes as stabilizer, Lot SHBJ7695
  - Primuline, SKU 206865-1G
  - THAP, Lot STBG4575V
- Honeywell Fluka, Fisher Scientific GmbH, Schwerte, Germany:
  - 2-Propanol, Chromasolv™ LC-MS, ≥99.9%
  - Acetic acid, ≥99.9%, Lot SZBG2450
  - Acetone, Chromasolv™, ≥99.9%
- Merck KGaA Germany
  - 9-aminoacridine, as-No: 90-45-9
  - Emsure® Acetonitril
  - Emsure® Ethanol
  - Emsure® Natriumchlorid, lot 106404.1000
- SERVA GmbH, Germany
  - Methanol for UHPLC-MS, Lot 181195
- Avanti® Polar Lipids, Alabama
  - 4ME 16:0 PC; 1,2-diphytanoyl-sn-glycero-3-phosphocholine

2.1.1 Other Equipment

- HPTLC Silica gel 60 A F254, aluminum plates by Merck Germany
- HPTLC Silica gel 60 RP-18 F254, aluminum plates by Merck Germany
- Micro Centrifuge Model SD by Roth, Germany
- Millipore Simplicity UV F2MA54197E by Molsheim, France
- Mini Vortex Mixer 444-2790 by VWR Leuven.
- SafeLock Tubes 0.5 ml by Eppendorf AG Hamburg, Germany, LOT J190277J
- SafeLock Tubes 1.5 ml by Eppendorf AG Hamburg, Germany, LOT I183019J
- SafeLock Tubes 0,5 ml by Eppendorf AG Hamburg, Germany, LOT J190277J
- Sonorex RK 100 by Bandelin, Germany

2.2 Sample Preparation

2.2.1 Biological samples

All samples were provided by our collaborator. Table 3 shows all samples used for the analysis. Apart from the parameters given, another difference in the samples is that in all TEL fermentations the biomass was taken over a longer period of time, whereas in the CC fermentations the samples were taken at a certain point in time.

Table 3: Details of the biological samples received, differing in growth temperature (GT), dilution rate (DR) and biomass concentration (BMC).

Sample	GT / °C	DR / h^{-1}	BMC /g/L
F3 TEL12 Bleed 6.1	75	0.01	1.95
F3 TEL12 Bleed 12	75	0.01	2.27
F3 TEL12 Bleed 13	75	0.01	2.14
F9 CC12 Sample 4	75	0.03	1.31
F9 CC12 Sample 9	68	0.01	1.62
F9 CC12 Sample 11	75	0.03	1.35
F9 CC12 Sample 16	82	0.01	1.77
F9 CC16 Sample 14	75	0.011	2.11
F9 CC16 Sample 15	75	0.035	1.95
F9 CC16 Sample 20	75	0.01	2.11
F9 CC16 Sample 23	75	0.035	1.85

The samples were obtained either as dry biomass, biomass dissolved in $CHCl_3$:MeOH (2:1, v/v), or biomass dissolved in dimethylsulfoxide(DMSO): isopropanol (2:3, v/v). Unfortunately no dates of the extractions of the respective samples' biomass could be provided. For better comparability, all samples analyzed directly by MALDI MS were diluted to a concentration of 33 mg/ml. The concentration of the samples for TLC measurements was adjusted according to the method. A protocol for dilution was developed for samples obtained as biomass.

Protocol:
The biomass is weighed in an Eppendorf SafeLock Tube and the amount of solvent is calculated depending on the weight to obtain a concentration of 33 mg/ml. The solvent used is $CHCl_3$:MeOH (2:1, v/v) which is added to the biomass in the safelock tube. Then the sample is placed on a thermoshaker at 38° at 600 rpm for one hour. This procedure is based on the dissolution procedure of our collaborator.

2.2.2 Sample preparation for MALDI MS

To be able to measure the samples with MALDI MS, they are mixed with suitable matrix mixtures. Most of our samples were measured using the matrix THAP. This matrix showed a good signal to noise ratio in both positive and negative ion mode. For all measurements the sample was mixed in the ratio 1:1 (v/v) with THAP dissolved in MeOH at 15mg/ml and vortexed for 15 seconds. For samples measured in positive ion mode, 0.5 mg NaCl was added to the 20 ml matrix sample mixture which saturated the solution. The mixture was then vortexed again. From that mixture 1.2 µL was spotted onto a stainless steel sample plate that is also called target. During the separation process by TLC, a certain part of the sample is lost. Accordingly, the signal to noise ratio also deteriorates when measuring the respective sample. The measurements with previous TLC separation were carried out on the Synapt G2 HDMS, which was still able to produce a good signal to noise ratio in positive ion mode, however, this was not the case in negative ion mode. For this reason, 9-aminoacridine (9-AA) was used for the negative ion mode measurements after TLC separation. This matrix generates only negatively charged ions, which is why only measurements in negative ion mode provide a signal. The sensitivity could thus be improved and a good signal to noise ratio could also be achieved in the negative ion mode. For the TLC measurements, 9-AA was used as a matrix for the negative ion mode in addition to THAP. This matrix, dissolved in isopropanol:acetonitrile (3:2, v/v) at 10 mg/ml, was also mixed 1:1 with the dissolved sample and 0.6 µL was spotted onto the target.

2.2.3 TLC Measurements

Protocol:
The TLC plates are cut into strips of 80 mm x 22 mm and as a first step a blank run is performed in 4 ml $CHCl_3$:MeOH (1:1, v/v), the plate is dried and the blank run is repeated. The blank run is performed in the same type of TLC chambers as the TLC separation, but in different chambers to avoid contamination. The chambers have a dimension of approximately 25 mm x 53 mm x 85 mm (width x length x height). The plates are then activated in an oven at 180 °C for 5 minutes. For the TLC separation, 8 spots of 0.5 µL sample each are spotted onto the silica gel plates in a row on 8 mm height with a glass capillary. This little amount of sample reduces the smearing effect and the multiple spots ensure a satisfactory signal during the measurement. A TLC chamber is filled with 5 mL of mobile phase to get a level of about 4 mm so the sample spots prior applied do not directly come into contact with the mobile phase. The mobile phase consisting of $CHCl_3$: MeOH : 90% AcOH (65:4:35) is left to stand for 30 minutes to ensure saturation of the chamber. Up to 8 TLC plates are then developed simulatneously until the front of the mobile phase reaches about 1cm below the upper edge of the plate. The TLC plates are then removed from the chamber and dried. A primuline solution, prepared according to the method of White et. al. [16], was applied to the plates by a simple spray mechanism and allowed to dry. The bands made visible under UV light were then scraped out and the scraped silica gel was collected in safelock tubes. Afterwards 60 µL of $CHCl_3$: MeOH (2:1) was added to the safelock tube to extract the lipids for 30 minutes in an ultrasonic bath. Afterwards, the silica gel was centrifuged and the supernatant was pipetted off. The supernatant was mixed in a 1:1 ratio with the corresponding matrix and spotted onto the target plate as described in chapter 2.2.2.

2.3 Synapt G2 HDMS Measurements

The instrument was calibrated with 5 mg red phosphorous suspended in 5 mL acetone [17]. The suspension was shaken before taking 1.5 µL and spotting it on the target plate. For all measurements the parameters were kept constant to ensure a certain degree of comparability.

- Positive and negative ion mode measurements
  - Laserpower 420 (a.u.)
  - Measurement duration of 60 seconds
  - Spiral measurement path across the target spot
  - Step rate 20 Hz
  - Mass range 800 to 2000 Da
  - Firing rate 1000 Hz

The polarity was the only parameter changed between positive and negative ion mode measurements. For MS/MS measurements, the manual mode was used and the duration of the measurement was adjusted in order to obtain a satisfactory signal.

- MS/MS measurements, positive and negative ion mode
  - Laserpower 420 (a.u.)
  - raster path across the target spot
  - Step rate 20 Hz
  - Mass range 50 to 2000 Da
  - Firing rate 1000 Hz

The trap collision energy was chosen, depending on the component to be analyzed, to obtain a good signal of the respective fragments. Depending on the component, this ranged from 85 to 105 (a.u.).

2.4 Spectra Analysis

Spectra measured on the Synapt G2 HDMS were converted into centroid spectra using MassLynx Software v4.1 for better comparison. For this purpose, the built-in function *Automatic peak-detection* was used and the parameters were kept at the default parameters the software uses. The measured spectra were analyzed and processed using Matlab. Background subtraction was performed on the representative spectra for structure analysis and component identification. For all spectra measured for comparative purposes, no additional processing was performed due to comparability. All calculations, plots and figures shown in this thesis were done with Matlab Version R2019b and QtiPlot version 0.9.9.7.

3 Results and discussion

3.1 Overview

The main aim of this master thesis was the identification of the components of *S. acidocaldarius* and the development of a technically reproducible normal phase TLC. In order to be able to compare measurements in a reasonable way, the measurement uncertainty has to be estimated. MALDI is not known for its quantification properties, however, the variability of our measurement process was determined in order to roughly compare samples. Furthermore, the behavior of the ring structures under different cultivation conditions was investigated.

3.2 Component Identification of *S. acidocaldarius*

The first measurements of the *S. acidocaldarius*' lipid extract in our research group yielded results with significant differences to those obtained in this master thesis.

On the one hand, the relative ratios of the components to each other differed, on the other hand Sulfono-Hex3-GDGT could not be detected. The initial measurements were performed on a Shimadzu Maldi 7090 TOF/TOF mass spectrometer.

During the analysis process of *S. acidocaldarius*, parameters in the cultivation process of the biomass changed repeatedly. To characterize these variations, ten different samples with varying production processes were measured and compared. Figure 15 shows the most recent sample F3 TEL12, bleed 13, from the final production process.

Looking at the measured spectra, there are a few peculiar features. The signal in positive ion mode is much stronger than the one in negative ion mode. Also, the ratios of the components to each other differ due to the different ionization probabilities in positive and negative mode. The components GDGT and Hex-GDGT are only visible in the positive ion mode because they do not contain sulfur or phosphorus and are therefore not ionized in the negative ion mode. In positive ion mode they can be detected due to their sodium adducts.

Since the measurements in positive ion mode shows a significantly higher signal in all measurements and since all components are visible in the positive ion mode, all analyses and comparisons are based on the positive spectra. The fact that a higher intensity spectrum is obtained in the positive ion mode than in the negative ion mode is due to several factors, including the tuning of the instrument, the choice of matrix and especially the addition of NaCl

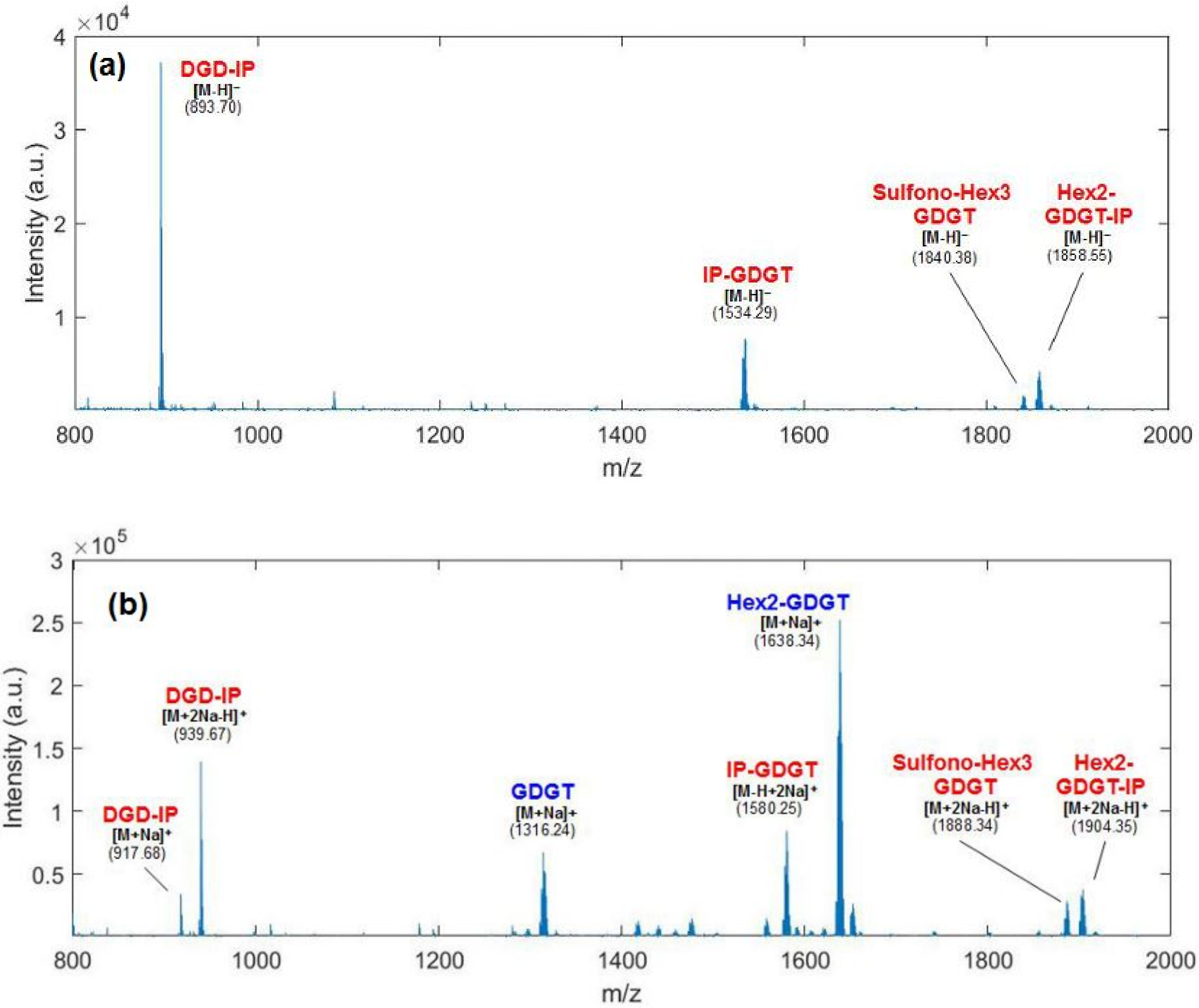

Figure 15: Spectra of F3 TEL12, bleed 13 in (a) positive and (b) negative ion mode, measured on Synapt G2 HDMS with THAP as Matrix. Components that could only be measured in positive ion mode are displayed in blue.

to the samples for positive ion measurements. It is also worth mentioning that the ratios of the individual lipids are not consistent between the different ionization modes which again is a result of different ionization properties of individual analytes. The masses measured compared to the calculated theoretical masses of the respective compounds are given in table 4.

The components that are present in our lipid extract show typical archaeal

Table 4: Lipid components measured in positive ion mode on Synapt G2 HDMS

Lipid species	Measured m/z	Theoretical m/z	Δ m/z	ppm
[IP-DGD 40;0 +2Na-H]$^+$	939.6637	939.6643	-0.0006	-0.639
[GDGT 80;4 +Na-H]$^+$	1314.2249	1314.2269	-0.0020	-1.521
[IP-GDGT 80;4 +2Na-H]$^+$	1580.2428	1580.2437	-0.0009	-0.570
[Hex2-GDGT 80;5 +Na]$^+$	1638.3322	1638.3326	-0.0004	-0.244
[Sulfono-Hex3-GDGT 80;5 +2Na-H]$^+$	1886.3275	1886.3294	-0.0019	-1.007
[Hex2-GDGT-IP 80;5 +2Na-H]$^+$	1902.3368	1902.3337	+0.0031	+1.630

membrane characteristics. Isoprenoid chains are bound to glycerol by ether bonds. The components can be roughly divided into two categories. Inositol phosphate dialkyl glycerol diether (IP-DGD) represents the first category. Two C_{20} isoprenoid chains which are bound to glycerol via ether bonds form the core structure. The head group, in our case, is always inositol phosphate (IP).

The second category is represented by glycerol dialkyl glycerol tetraether (GDGT). They consist of two C_{40} isoprenoid chains which are bound to glycerol on both sides. This core structure can bind different head groups and form different numbers of cyclopentane rings. [18] In 2014 Sara M. et al Jensen studied a species related to *S. acidocaldarius*, *S. islandicus* [18]. The lipid components of these two species are well comparable and the identification in this thesis is based on the work of this group. A detailed structure of the lipids can be found in the appendix, shown in figure 38 and figure 39.

3.2.1 MS/MS Structural Analysis

In order to confirm that the lipids in our biomass are indeed the components we have assigned, MS/MS measurements were performed. First, IP-GDG was fragmented to check if an isoprenoid structure can be observed. The spectrum shown in figure 16 was recorded on the Shimadzu MALDI 7090 because it can provide a lot more energy, up to 20 keV, to an analyte ion for fragmentation.

Due to CRF, fragmentation occurs at the CH_2 groups located far away from the charge of the ion. However, both bonds at the methylene branching points are never fragmented simultaneously, since this is unfavorable from an energetic point of view. The fragments of IP-GDG show regular mass differences of about 14 Da corresponding to the loss of one CH_2 group each. In addition, the periodic intervals of 28 Da, which are typical for isoprenoid chains and always indicate a branching point in the molecule, are visible.

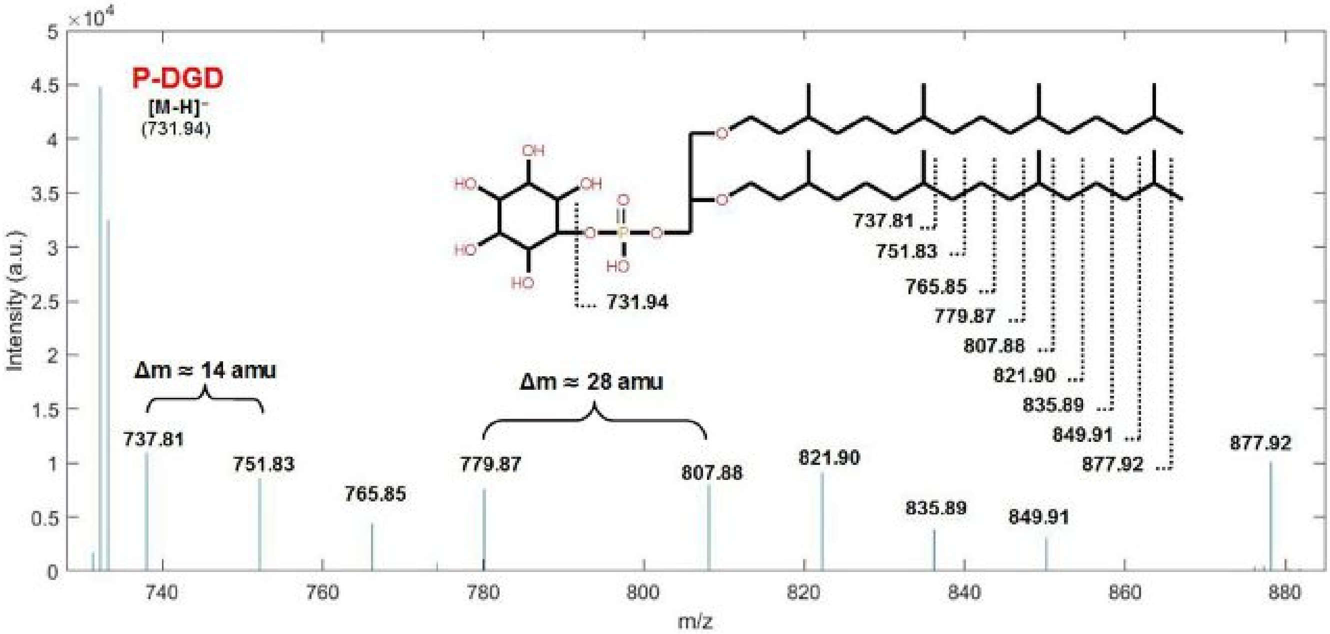

Figure 16: Fragmentation pattern of IP-DGD, measured on the Shimadzu MALDI 7090 with THAP as a matrix.

Sulfono-Hex3-GDGT could not be detected in the initial measurements, which were performed on the Shimadzu MALDI 7090 prior to the start of this thesis. This is not an issue of the instrument, as Sulfono-Hex3-GDGT could be observed also on the Shimadzu MALDI 7090 in measurements of samples received for this thesis, but most likely due to changes in the production process between the samples of the initial experiments and the samples received for this thesis. To confirm that this component is indeed Sulfono-Hex3-GDGT, an MS/MS measurement was performed. The characteristic ions could be detected, as shown in figure 17.

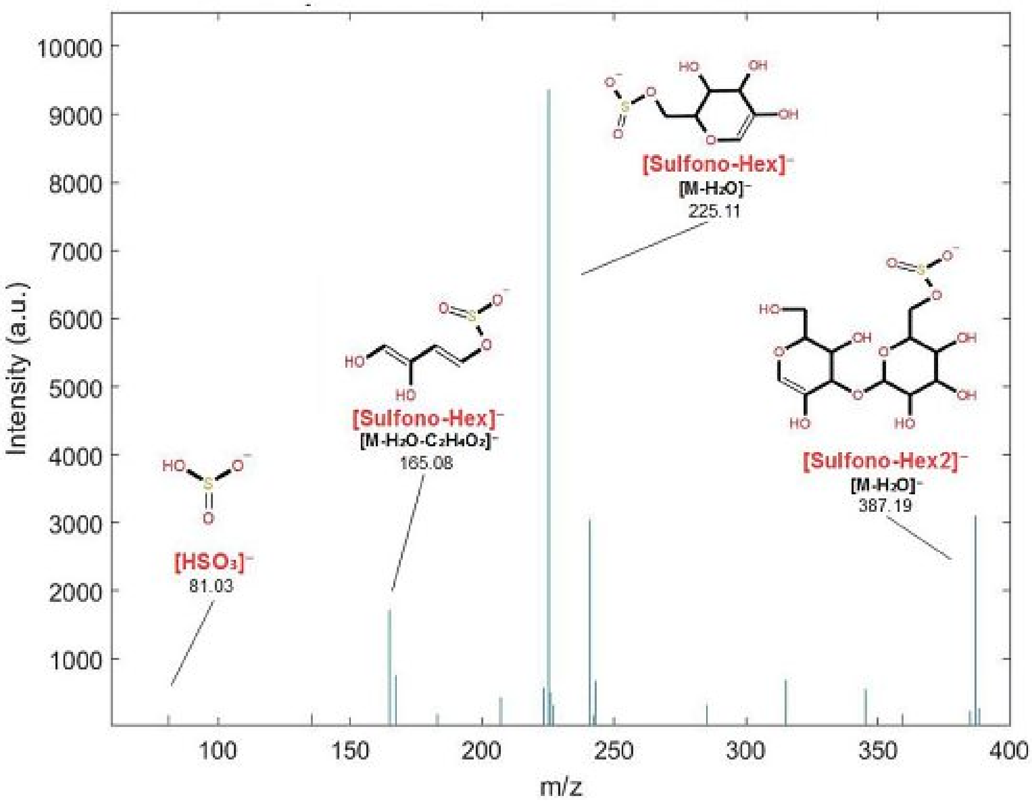

Figure 17: MS/MS spectrum of Sulfono-Hex3-GDGT, measured on the Synapt G2 HDMS with THAP as a matrix.

Since the mass difference between Sulfono-Hex3-GDGT and Hex2-GDGT-IP is very small, the ions could not be fully isolated in the MS/MS experiments. The reason being, that the instrument not only allows ions with the exact m/z value - selected for the precursor ion - to pass the first mass analyzer, but also allows a narrow distribution of ions around the selected m/z value to pass. However, this distribution was not narrow enough to allow only Sulfono-Hex3-GDGT to pass without also passing Hex2-GDGT-IP ions while maintaining a good signal-to-noise ratio. By default, the m/z value for the precursor ion for Sulfono-Hex3-GDGT was set to 1884 Da. This setting provided a good signal to noise ratio, but the fragment ions of Hex2-GDGT-IP also appeared in the spectrum. Subsequently, the m/z value of the precursor ion was decreased in steps of 2 Da until an m/z value of 1874 Da was reached, which did not provide any signal at all. The signal to noise ratio dropped steadily, but isolation was still not achieved until the signal became too weak. For this reason, 1884 Da was retained as the m/z value of the precursor ion. Figure 18 shows the fragment spectrum of Hex2-GDGT-IP which could be better isolated.

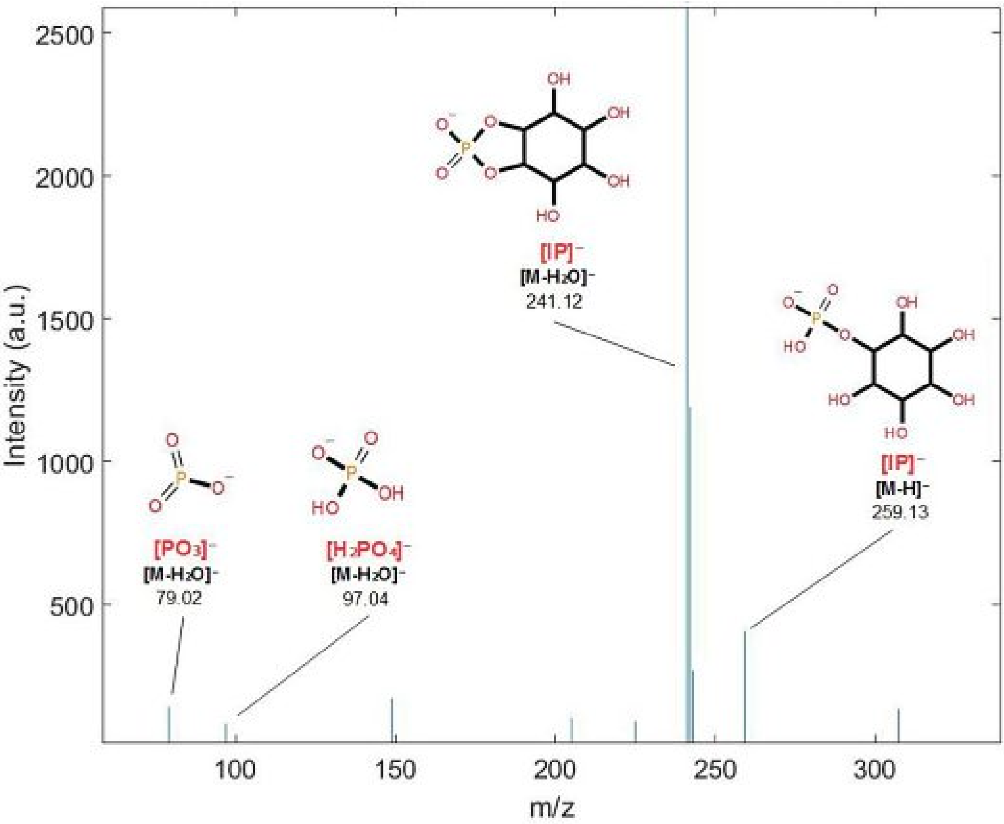

Figure 18: MS/MS spectrum of Hex2-GDGT-IP, measured on the Synapt G2 HDMS with THAP as a matrix.

Additionally MS/MS measurements were performed to show the decay patterns of Hex2-GDGT fragmenting into Hex-GDGT and GDGT, and IP-GDGT fragmenting to P-GDGT and finally GDGT.

3.2.2 Pattern Calculations

The isotope distribution of the components of *S. acidocaldarius* looks quite unusual at first sight. The membrane lipids of *S. acidocaldarius* have the peculiarity to form different amounts of cyclopentane rings in their isoprenoid chains, depending on the cultivation conditions. By formation of a cyclopentane ring the lipid loses 2 hydrogen atoms. Therefore its molecular mass is reduced by 2 Da. The unusual distribution of the peaks measured represents a superposition of the same lipid with a different number of cyclopentane rings. Up to 7 rings were found in the lipids investigated.
An algorithm was developed in Matlab to describe the ring distribution. It calculates the proportion that lipids of different amount of cyclopentane have in the spectrum. The algorithm is provided in the appendix in chapter 6.5. In order to perform such a calculation, the measured spectrum must display a true isotopic pattern. The Synpat G2 HDMS, on which all spectra used for the pattern calculation were measured, fulfills this requirement. For the calculation, the signal is first transformed into a centroid spectrum. Then, the isotope distribution of the respective molecules, the peak positions and signal intensities are transferred to the algorithm. The calculation starts at the molecule peak with the most cyclopentane rings. This is the peak of the lipid with the least hydrogen and therefore the lightest of all peaks, it is not overlaid by any other component. The calculation is based on the monoisotopic peak for GDGT. For IP-GDGT, Hex2-GDGT, Sulfono-Hex3-GDGT and Hex2-GDGT-IP it is based on the first isotopic peak M+1. These peaks are the most intense ones due to the isotope distributions of the respective components and considering them as starting point minimizes the calculation error. For every component the respective theoretical isotope distribution is scaled to the particular peak's intensity. The calculated distribution is subtracted from the original spectrum. In the newly obtained spectrum, the proportion of the lipid with one less ring is calculated in the same way. This is repeated until all lipids of different cyclopentane amount are characterized. Due to this calculation method a propagating error can not be avoided, however it can be neglected due to the predominant measurement uncertainty associated with the MALDI-TOF measurement. Furthermore, due to the nature of the algorithm calculating the proportions from lower to higher m/z values, a propagating error leads to a larger deviation of the calculation in the proportions of lipids with fewer cyclopentane rings. The other error which has to be taken into account is the fact that the calculated proportions are peak intensities starting from the most intensive one. However, m/z intensities are depending on ionization efficiencies. Yet, these intensities are to some extent fluctuating introducing a certain inaccuracy.

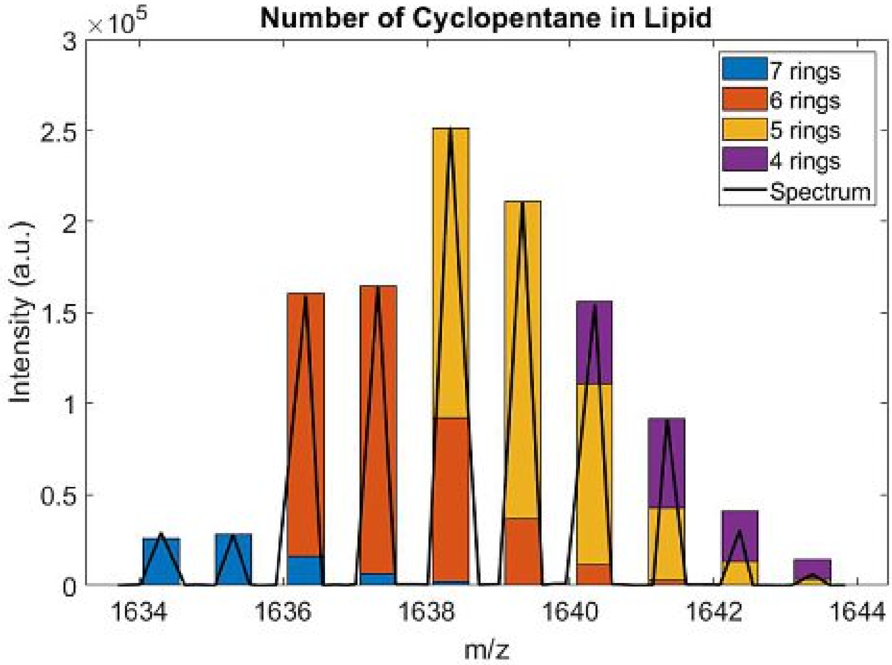

Figure 19: Calculated cyclopentane distribution in Hex2-GDGT from a representative sample overlaid with the measured centroid spectrum .

In figure 19, an example of a superposition calculation is shown. The bars of different colors each correspond to a scaled theoretical isotope distribution. The ring distribution can be calculated by shifting the isotope distributions by 2 Da and scaling it with the original signal. The information obtained by the algortihm can further be used to calculate the average ring number. Due to statistical variations in the measurement, the spectrum does not exactly match the calculated distribution. For intensities below 10^3 a.u. on the synapt G2 HDMS the average calculation error is about 8.4%. The better the signal, the more precisely the superposition is matched and statistical fluctuations lose influence. For intensities above 10^3 a.u. on the synapt G2 HDMS the average relative calculation error is about 1.8%.

3.3 Thin Layer Chromatography

An essential part of this work was the development of a fast separation method of the lipid extract's components by TLC. A normal phase TLC method was developed which allowed to separate the lipids into three groups. Since the separation is based on head groups and most of the polar lipids of the extract contain IP as head group, a more precise separation by normal phase TLC is not possible.

That is why an attempt was made to develop a reversed phase TLC method. However, it was found that no mobile phase, regardless of its polarity, could be used to separate the lipids. Instead the lipids stuck to the site of application. Since no more precise information could be obtained from the manufacturer, it was assumed that the silica gel on the reversed phase TLC plates was not end-capped and therefore bound to the lipid's free OH groups, making it impossible to separate and elute the sample from the TLC plate. Since no end-capped silica gel RP-TLC plates were available for purchase, the system was switched back to NP-TLC plates. For NP-TLC, all mobile phases tried gave a separation of the sample into 3 bands. The mobile phases investigated with the respective stationary phase and the separation of the lipids obtained are shown in the appendix in chapter 6.2. However, the best separation was obtained with the method which is based on the archaea studies conducted by R. Angelini [19]. It was found that the separation worked very well and consistently. Figure 20 shows a TLC plate developed with this method. However, two problems arose, a weak signal intensity and a smearing effect showing insufficient separation. To improve signal intensity the scraped off silica gel of four samples scraped of the TLC plate was pooled. Increasing the number of samples resulted only in poorer signals.

The more lipid extract was applied to a single spot on the TLC plate, the better the signal was. However, this also resulted in increased detection of Hex2-GDGT, GDGT and DGD-IP in all three bands. It was observed that the spotting of 0.5 µl was the best compromise between a sufficient MS signal and a good separation, as described in detail in chapter 2.2.3. Spotting less than 0.5 µl per spot made it impossible to stain the first of the three bands with primuline, as it contained less analyte than the other bands and was not easily detected even at 0.5 µl per spot.

A smearing effect occurred at 0.5 µl. Furthermore the skill of the operator influenced this smearing effect because on the one hand the glass capillaries had marks only at integer microliter values, on the other hand the spotting of an exact volume was also difficult for volumes larger than 0.5 µl because the mixture left the capillary quite fast when it was placed on the TLC plate. Therefore it was difficult to assure that each spot contained exactly 0.5 µl of

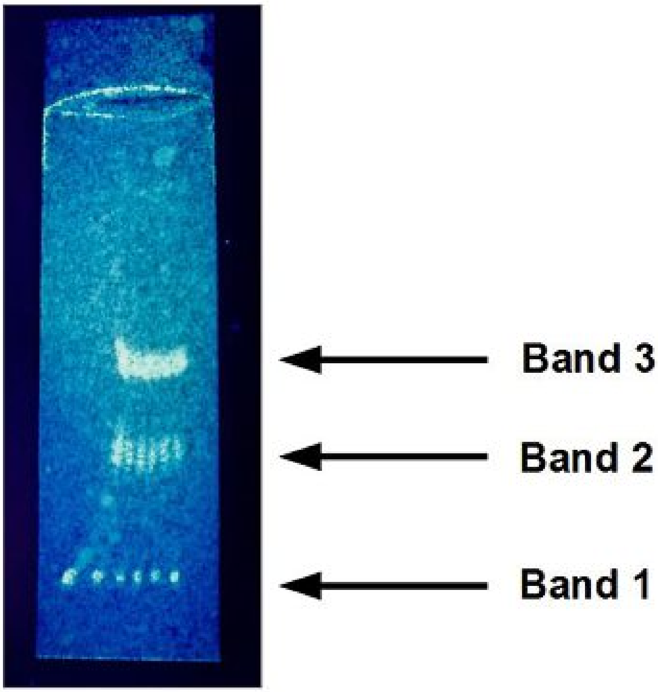

Figure 20: A developed TLC plate stained with primuline, photographed under UV light of wavelength 365 nm.

sample-mixture. Thus a slightly stronger or slightly weaker smearing effect could occur for different separations. Repeated measurements under otherwise identical conditions showed that the spotting had no major impact on the measurements.
The measurement of the components after TLC separation is still very errorprone since sample losses must be expected in every step of TLC development. Especially the extraction of the lipids from the silica gel can lead to high sample losses. To estimate these losses, a MS-standard, 1,2-diphytanyl-sn-glycero-3-phosphocholine (PC) dissolved in MeOH at a concentration $2g/l$, was measured with and without TLC separation. Measurements were performed according to the TLC protocol for the lipid extract. The measurement results are shown in figure 21. Three plates were pooled and 5 spots of 2 µl each were spotted on the TLC plates. The concentration of the standard was $2g/l$ in both measurements. The measurement in figure 21a shows a signal three times stronger for the pure standard than the standard developed by TLC, shown in figure 21b. Since three plates with 5 spots each were pooled,

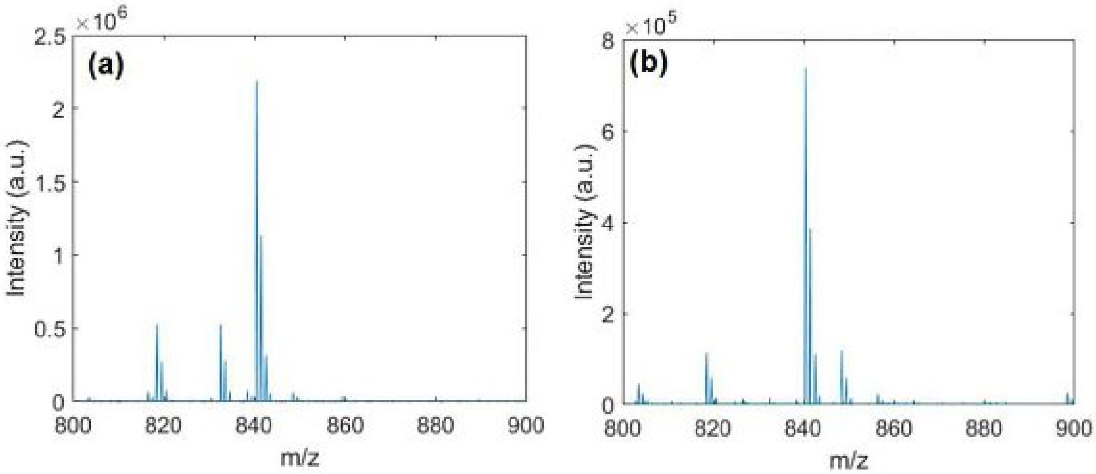

Figure 21: Measurement of PC (a) according to Synapt G2 measurement protocol and (b) after TLC separation and extraction from the stationary phase.

i.e. in total 5µl sample were applied 15 times on the TLC plates, the signal after TLC development was weaker by factor k=45. This factor is only a rough estimation since the fluctuations in signal intensity does not allow exact predictions in this case, as the results of the quantification measurements show. Since it can not be assumed that the distribution of the lost components is always constant, the ratios of the components to each other in the measured spectrum may differ. During the work with the TLC method it was found that the Synapt G2 HDMS has a lower sensitivity in negative mode than in positive mode. In some cases, the TLC measurements in negative mode could not provide a satisfactory signal. For this reason, the matrix was switched from THAP to 9-AA for the TLC measurements in negative mode, as described in subsection 2.2.2. Comparison measurements of THAP and 9-AA, shown in figure 31, showed a significant improvement of the signal with 9-AA, but only in the negative mode, as described in literature [20].

As for THAP, a background measurement of 9-AA and the TLC plate was performed. For this purpose, silica gel was scraped from a TLC plate that was developed in the same chamber but did not contain sample spots. This way, any impurities that might have been present in the TLC chamber could also be taken into account. Table 5 shows the components measured in the respective bands. The first band contained the lipids which have different functional groups but a similar molecular mass. Hex2-GDGT-IP and Sulfono-Hex3-GDGT always co-migrated and were detected in band 1. Changing the

Table 5: Components measured in the respective bands with their R_f value.

Band	Components	R_f
Band 1	Sulfono-Hex3-GDGT, Hex2-GDGT-IP	0.08
Band 2	GDGT-IP, DGD-IP, GDGT-P	0.38
Band 3	GDGT, Hex-GDGT, Hex2-GDGT	0.55

mobile phase had no influence on this behavior. All other lipids which had IP as a headgroup are found in band 2. Due to the fact that GDGT, Hex-GDGT and Hex2-GDGT appeared in band 3, only positive ion mode measurements yielded a result for this band.

3.4 Analytical considerations

3.4.1 Comparison of Instruments

In order to exclude systematic errors caused by the Synapt G2 HDMS, a sample was measured on two other instruments and the spectra were compared. All instruments used MALDI as ionization method, but differed in their mass analyzers as well as IP-MALDI versus vacuum MALDI. Since many factors were involved in the measurement signal and the measurements at the Synapt G2 HDMS were not consistent in itself, the spectra can only be roughly compared to each other. As can be clearly seen in figure 22, the spectra vary greatly among each other. The intensity fluctuation of GDGT in particular is very significant. IP-GDGT also shows a significant variation in its ratio to the other components. The fluctuations could be due to the high laser power used. The scimaX measurement was done with 22% laser power, the Shimadzu MALDI 7090 with 76%, and the Synapt G2 HDMS, in order to compare the samples to other measurements, as usual with 420 (a.u.) laser power corresponding to 84% of its total laser power. The higher the amount of GDGT, the lower the amount of IP-GDGT seems to become, which may be an indication for in-source fragmentation and also an indication that IP-GDGT is the respective precursor ion. Comparing the laser power of different instruments is problematic to a certain extent, since it is strongly dependent on the age of the laser and the number of laser shots taken prior to the measurements on every respective instrument. In addition, the required laser power is also dependent on the sensitivity of the instrument. The more sensitive an instrument, the less laser power is required for the measurement of the lipid sample and consequently the lower the unwanted fragmentation of the components. Nevertheless, the measurement on the scimaX, which has the highest sensitivity of the three instruments, shows a very small proportion of GDGT in the spectrum which is very likely to a lower laser power used in the measurements, reducing the issue of unwanted in-source fragmentation that is appearing to be a problem on the other instruments used and further discussed in chapter 3.4.2.

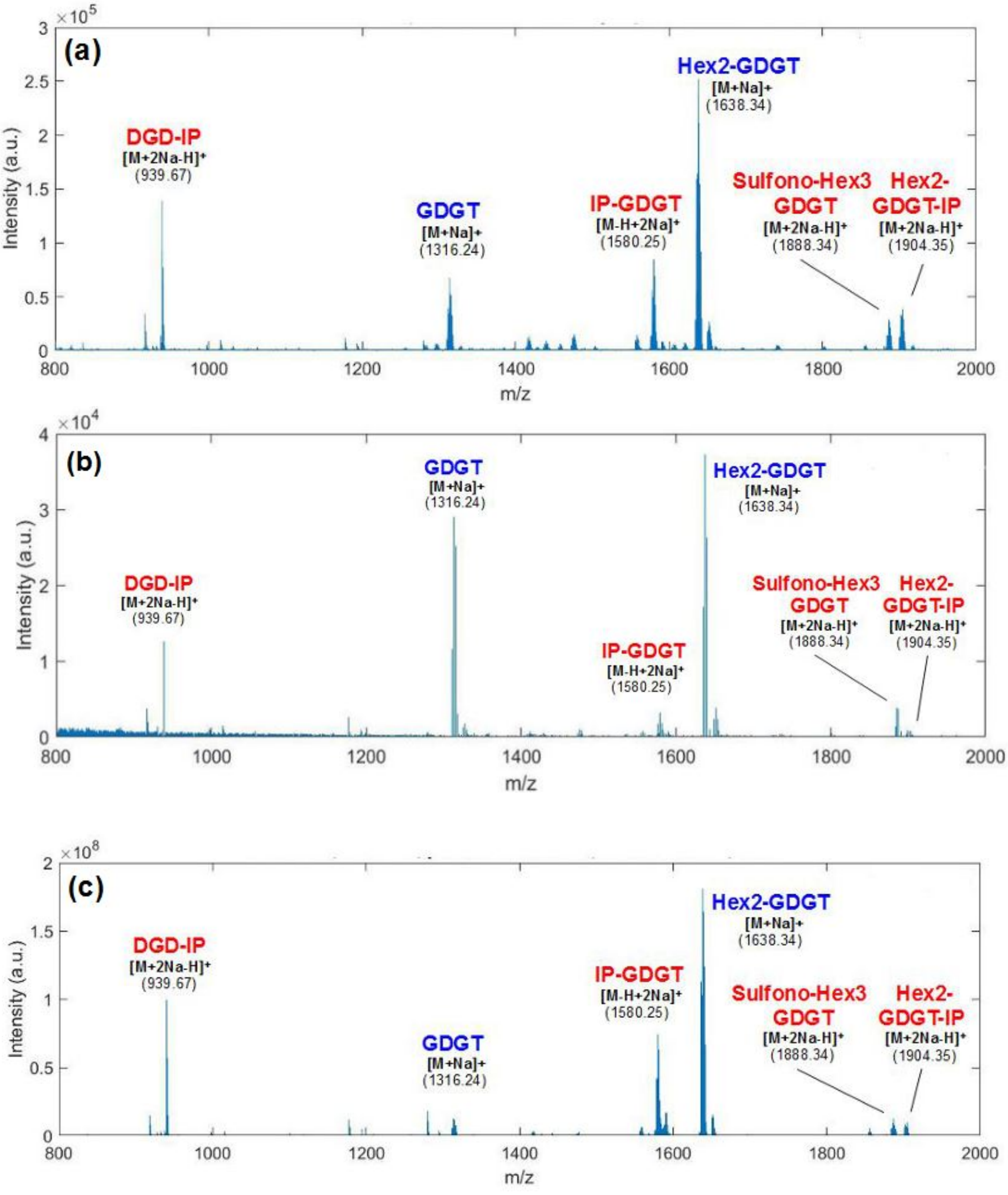

Figure 22: F3 TEL 12, bleed 13, measured on (a) the Synapt G2 HDMS, (b) the Shimadzu MALDI 7090 and (c) the scimaX in positive ion mode using THAP as a matrix.

Looking at the negative ion mode spectrum shown in figure 23, variations in the ratios of the components can be seen as well. A dominance of Sulfono-Hex3-GDGT in the spectrum of the Shimadzu MALDI 7090 is especially noticeable which seems to be related to the matrix used. The matrix 9-AA seems to preferentially ionize the components Sulfono-Hex3-GDGT and Hex2-GDGT, this phenomenon shows up on both instruments in different strength, which will be further discussed in 3.4.6.

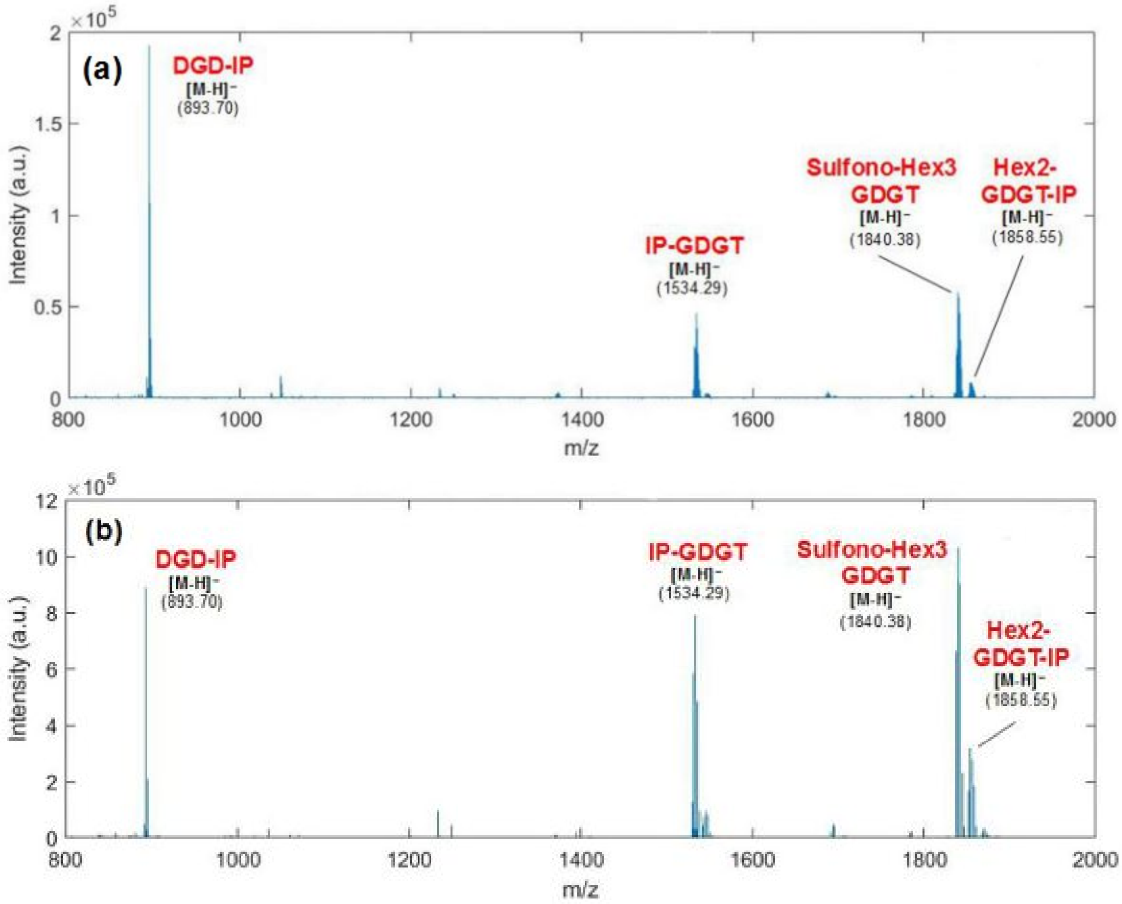

Figure 23: F3 TEL 12, bleed 13, measured (a) on the Synapt G2 HDMS and (b) on the Shimadzu MALDI 7090 in negative ion mode with 9-AA as a matrix.

3.4.2 Influence of Laser Power

The choice of laser power plays an important role. A strong signal with high mass resolution and high absolute intensity to minimize statistical fluctuations and improve the signal-to-noise ratio is wanted. Obtaining the best signal possible is obviously also very important for measuring low abundant analytes. MALDI-MS measurements of lipids obtained after TLC extraction are accompanied by a loss of ionization effects decreasing the absolute signal intensity, required a much higher laser power to obtain a satisfying signal. However, an increase in laser power leads to increased in-source fragmentation of lipids making identification of the actual sample compound difficult or even impossible. This holds particularly true in the case of *S. acidocaldarius* since all of the main components belong to one genus, possibly leading to a fragmentation induced intensity shift in the measured signal.
At this point, the question arises to what extend the intensity ratios of our components are true and whether a significant portion of the lighter component's signal originates from fragmentation of the larger components. Evaluations of the TLC bands showed a certain pattern which is at least partly due to the high laser power.

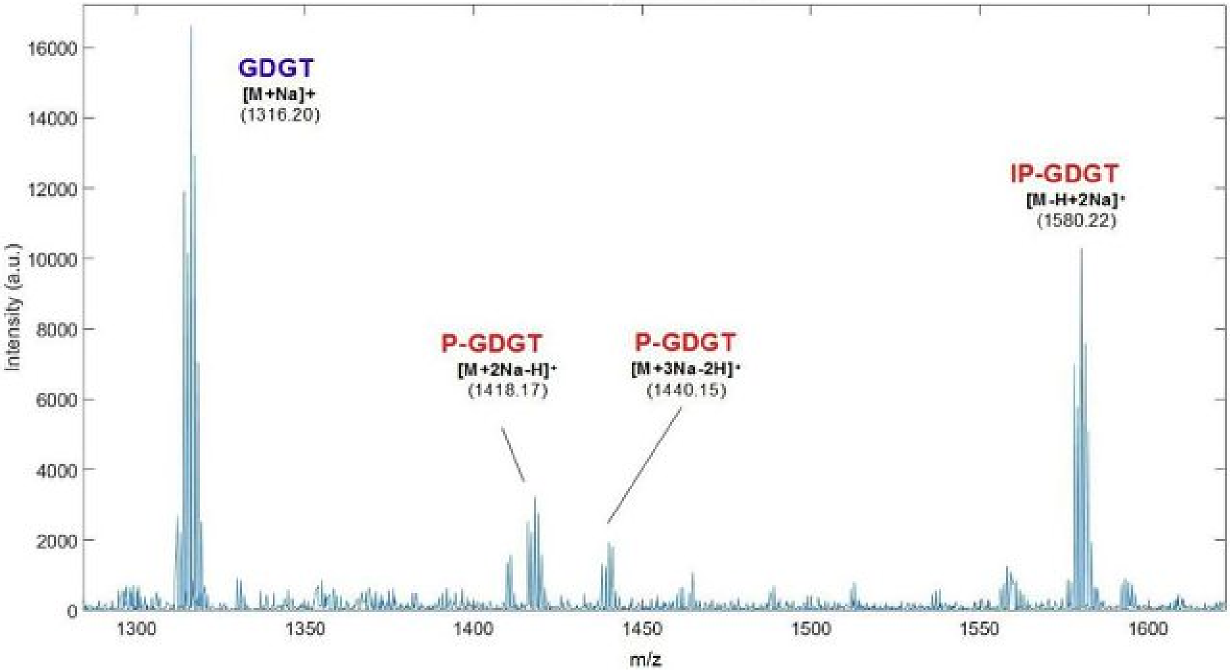

Figure 24: A section of the measurement of lipids extracted from band 2 after TLC separation in positive ion mode, measured on the Synapt G2 HDMS with THAP as matrix.

In figure 24, a zoom into the mass spectrum of the lipids extracted from band 2 is shown, measured in positive mode. The pattern is most likely caused by IP-GDGT acting as precursor ion. This pattern is common to all TLC separations, but it is necessary to estimate which part of the peaks in the spectrum is caused by the unavoidable smearing effect during chromatography and which is caused by fragmentation.
To quantify this fragmentation induced intensity shift, the entire lipid extract was measured with different laser powers and the ratios of the components to each other were examined. Since the TLC samples provided a relatively weak signal, the calculations were based on a spectrum were all studied components were present. The disadvantage of this method is, of course, that several lipids can act as a precursors for other components. In the case of GDGT, four of our main components can act as precursor ion and it is not possible to determine how much of the fragmented GDGT is made up of which component. The ratio of the intensity of GDGT to all four possible precursor ions is shown in figure 25a.

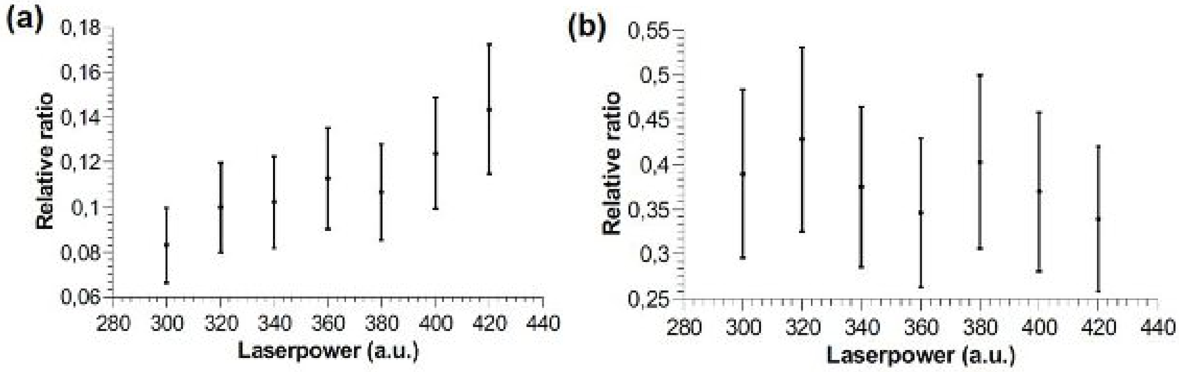

Figure 25: The relative ratios of (a) GDGT to $\sum_{i=1}^{4}$ precursor(i) and (b) IP-GDGT/Hex2-GDGT.

This data implies that the ratio of GDGT compared to the other components increases strongly with increasing laser power. It can be argued that this behavior could have many causes. Especially the different ionization probabilities of the components in dependence of the laser power could have a huge influence on these ratios and cannot be determined with a large statistical uncertainty like the one in our measurements.
Taking a look at the ratio of IP-GDGT to Hex2-GDGT in figure 25b, no such trend is seen. Hex2-GDGT does not fragment into IP-GDGT and the ionization mechanisms and therefore the probability of ionization of these two can be considered to be very different, yet their ratio to each other does

not change significantly with laser power variation.
Considering the ratio between GDGT and Hex2-GDGT, shown in figure 26a, where both components can be considered to have a very similar probability of ionization, the same trend as in figure 25a can be seen with increasing laser power.
In conclusion, it can be stated that a varying laser power does not seem to have a significant effect on the change in ionization probability of the studied components which have different ionization mechanisms and therefore assumably different ionization probabilities,like IP-GDGT and Hex2-GDGT, as the data in figure 25b implies. However, the ratio of two components having similar ionization mechanisms and therefore similar ionization probabilities, like GDGT and Hex2-GDGT, apparently shows a very strong dependence of the laser power variation, as the data in figure 26a implies.
Combining the findings from figure 25b and figure 26a it can be concluded that the shift in intensities is, to a very large extent, induced by fragmentation. It strongly outweighs a possible shift in intensities resulting from laser power-dependent changes in the ionization probabilities of the respective components.

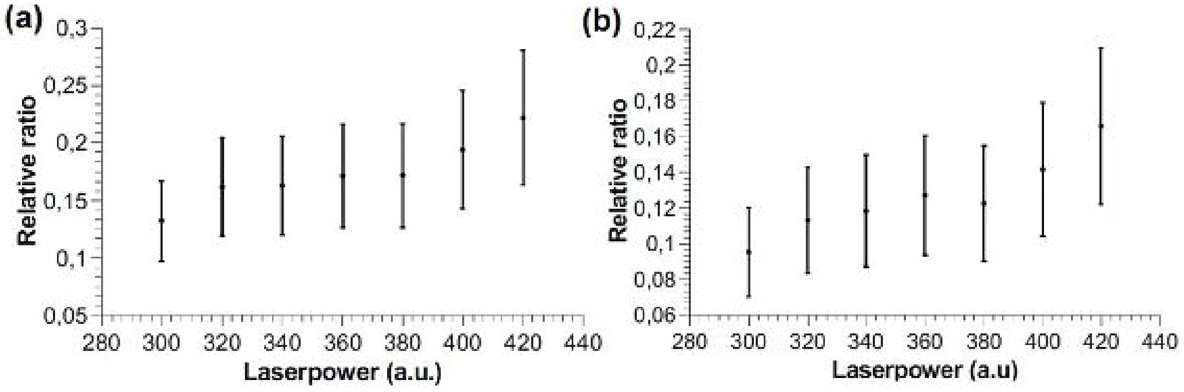

Figure 26: The relative ratios of (a) GDGT to Hex2-GDGT and (b) GDGT to (IP-GDGT + Hex2-GDGT).

Since the ratios of GDGT to Sulfono-Hex3-GDGT and to Hex2-GDGT-IP do not vary significantly, and because of their relatively low abundance in the spectrum, it can be assumed that most of the fragmented GDGT comes from the two more intense components Hex2-GDGT and IP-GDGT. That is why the data shown in figure 26b is used to estimate a correction factor of GDGT. A calculation of a correction factor for the intensity of GDGT is not considered practical because the uncertainties in the measurements are too big. However, figure 26b shows a reduction of the intensity of GDGT of about 40% at a laserpower of 300 (a.u.). This value should not be considered exact, but rather a rough estimation. Measurements with a laser power less than 300 (a.u.) did not yield a satisfactory signal-to-noise ratio to perform representative calculations. It must be noted that there is a very high measurement uncertainty. Therefore, a significant deviation due to fragmentation processes can only be determined for GDGT. Although MALDI is considered a gentle ionization method, we have to set the laser power to high values, by this a significant portion of our lipids fragment during the ionization process. Due to the high number of unknowns and the high uncertainty it is not reasonable to create an exact model of this process, but an approximate quadratic dependence can be seen from a laser power of 380 (a.u) upwards. The fragmentation process probably starts to dominate the distribution at this point. The fragmentation process seems to be of significant relevance only for GDGT due to its 4 possible precursor ions in the lipid extract. It is therefore neglected for the other components as it is within the range of measurement uncertainty and cannot be estimated.

3.4.3 Technical Reproducibility

The TLC separation method was developed to be used as a quick control method of the lipid production process in the near future. Therefore, it is important to be able to provide reproducible results. To confirm whether this is the case, the lipid extract sample F3 TEL12, bleed 13, was separated by TLC and measured on the Synapt G2 HDMS on three different days and the results were compared to each other, shown in figure 27.

The remaining spectra can be found in the appendix in section 6.4. Comparing the measurements of the three days, it can be seen that the contained components are always the same. The intensity and the proportions fluctuate quite strongly in some cases. Due to the in-source fragmentation discussed in the chapter 3.4.2, components are also visible in the spectra of the individual TLC bands, especially in the positive ion mode, which should not actually contain these components. In band 1 this is Hex2-GDGT, which is formed by fragmentation of Sulfono-Hex3-GDGT and Hex2-GDGT-IP, in band 2 it is mainly GDGT. The unpreventable smearing effect on the TLC plate is superimposing the mass spectra originating from fragmentation, resulting in a mixed mass spectrum of actual compounds and measurement artifacts. Band 3 provides a signal for measurements in positive ion mode only because the components present in band 3 do not ionize in negative ion mode.

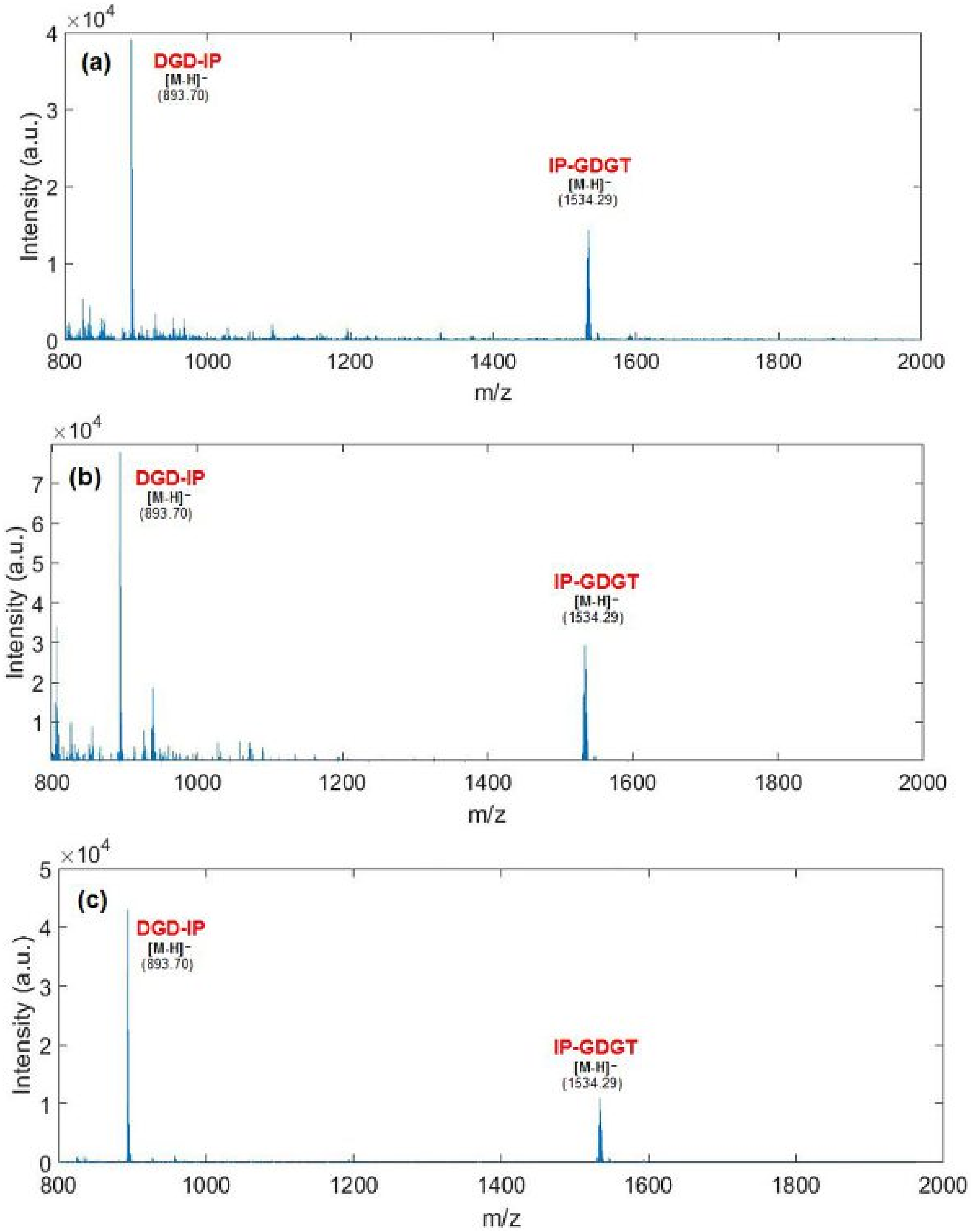

Figure 27: Measurements of lipids extracted from band 2 of four developed TLC plates measured on Synapt G2 HDMS with THAP as a matrix. Each of the three TLC developments and associated measurements was carried out on a different day under the same conditions.

The fragmentation of the components cannot be reduced by using less laser power since the signal intensity of the less abundant lipids is strongly influenced by this and a uniform laser power is used as a basis for comparison. The spectra of the measurements after TLC separation show that in band 1 a significant fraction of Sulfono-Hex3-GDGT and/or Hex2-GDGT-IP fragments into Hex2-GDGT at laser power 420 (a.u.). It cannot be determined what fraction of Hex2-GDGT originates from which of the two possible precursor ions and which part of the signal originates from a smearing effect in the TLC plate.

For the spectrum of band 1 this means that the intensity of Hex2-GDGT should not be as high as it appears in the measurements and consequently a part of Hex2-GDGT measured in every sample is likely to be a fragment of either Sulfono-Hex3-GDGT or Hex2-GDGT-IP. However, since this fraction is not significant with regard to the measurement uncertainty, the estimation of a correction factor is omitted.

3.4.4 Comparison of Solvents

The samples obtained after fermentation were dissolved in different solvent compositions. By default, the lipid extract was dissolved in $CHCl_3$:MeOH (2:1, v/v). Some samples obtained were dissolved in DMSO:isopropanol (2:3, v/v). This was more convenient for the liposome production, but made analysis by MALDI more difficult. DMSO has a very high boiling point, therefore a sample dissolved in DMSO and mixed with a matrix does not crystallize on the target, because the solvent does not evaporate. To avoid this problem, the sample was diluted 1:9 with $CHCl_3$:MeOH (2:1, v/v) to reduce the DMSO content and allow the matrix to crystallize. The remaining DMSO volatilized in the vacuum of the instrument. It is possible that the selected solvent changes the measurement results. In order to estimate this effect, the same sample dissolved in $CHCl_3$:MeOH (2:1, v/v) with the same lipid extract concentration was obtained and diluted in the same way with $CHCl_3$:MeOH (2:1, v/v) in a ratio of 1:9 to check the influence of the solvent. All components were present in the sample dissolved in DMSO:isopropanol (2:3, v/v) in the same way, only the proportions of the lipids varied, as figure 28 shows. Whether this variation was due to the solvent or due to the standard measurement uncertainty, could not be clearly shown. However, it appears that the lighter components GDGT and IP-DGD are not dissolved as well in DMSO:isopropanol (2:3, v/v) as in $CHCl_3$:MeOH (2:1, v/v), or that the other components are better dissolved in DMSO:isopropanol (2:3, v/v).

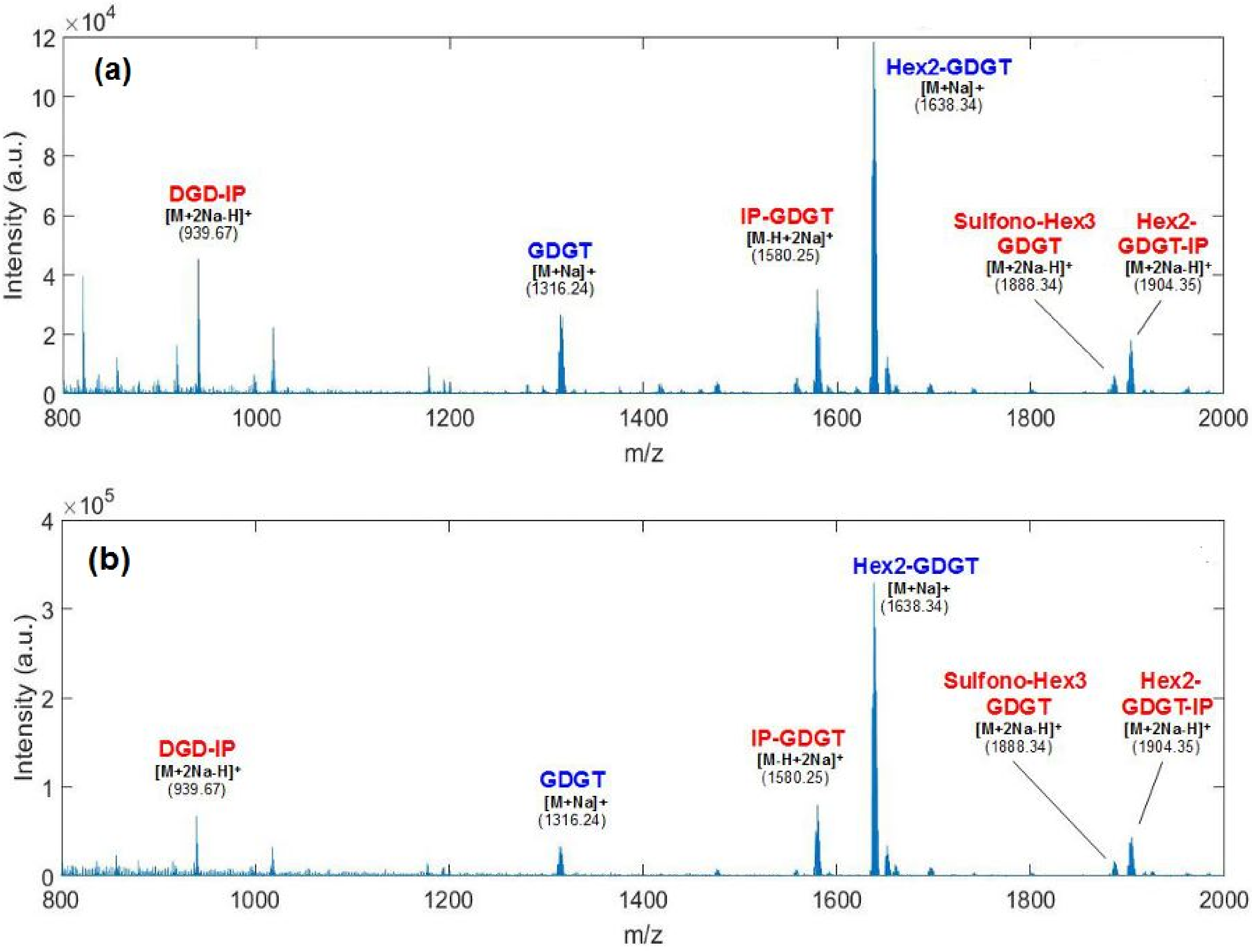

Figure 28: Comparison of a representative sample dissolved in (a) $CHCl_3$:MeOH (2:1,v/v) and (b) DMSO:isopropanol (2:3, v/v). Both samples were diluted with $CHCl_3$:MeOH (2:1, v/v) in a ratio of 1:9 to ensure comparability.

3.4.5 Biological Reproducibility

The first measurements of the lipid extract in our group were carried out before the start of this thesis. The spectrum measured differs in some respects from the current measurements which is due to the fact that the production process of the lipids was subject to constant optimization. Production parameters were changed and thus influenced the lipid extract.

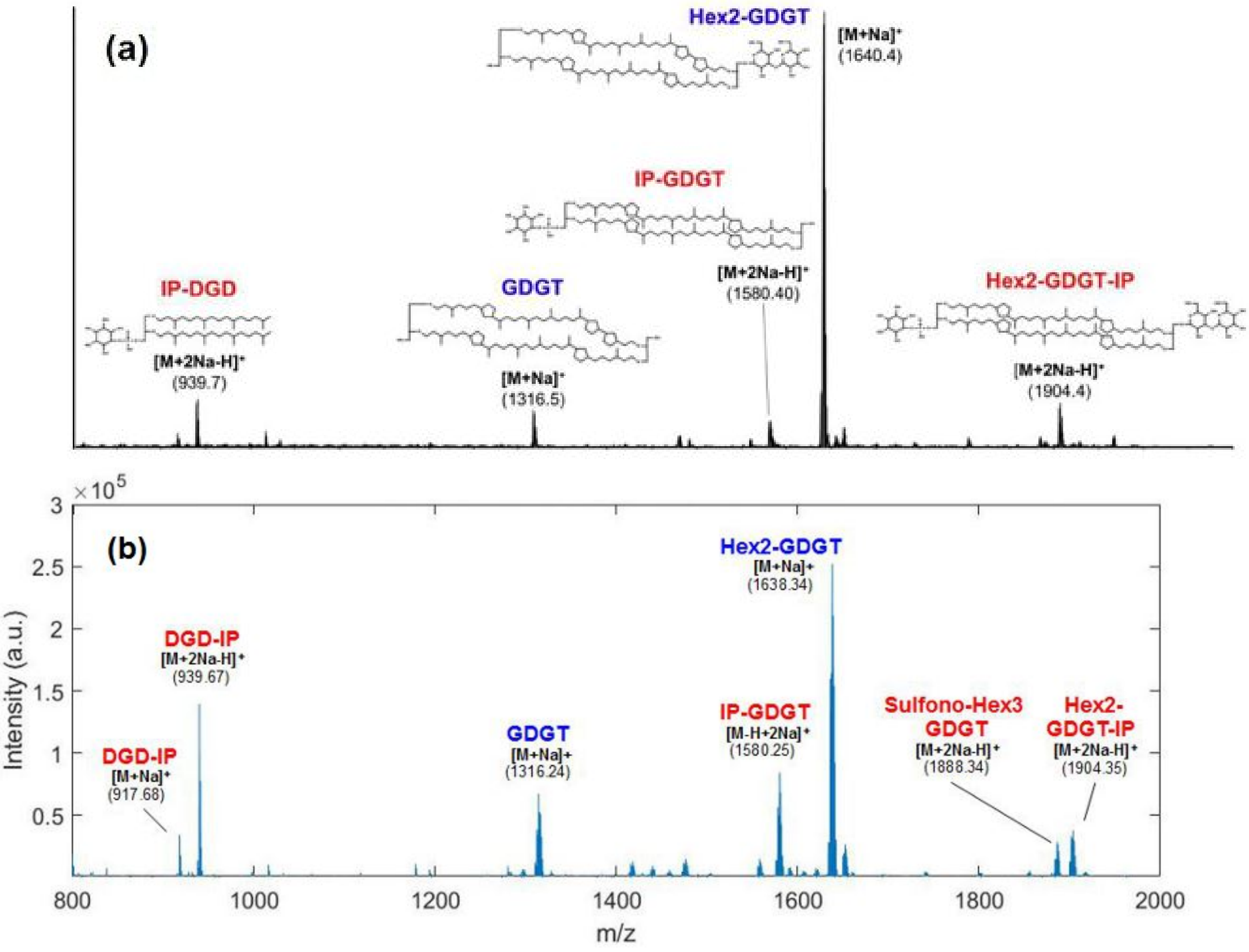

Figure 29: Comparison of different samples: (a) positive ion mode measurement on Shimadzu 7090, adapted from [3]; (b) positive ion mode measurement on Synapt G2 HDMS, both using THAP as a matrix.

The spectrum of more recent samples show a clear signal for Sulfono-Hex3-GDGT compared to the earlier measurements where this component does not seem to be present, as shown in figure 29. The clarification if this lipid was present was very important for the adjustment of the parameters of the fermentation. Therefore structural analysis was performed on this sulfoglycolipid. Furthermore, Hex2-GDGT does not appear to be as dominant as in the initial measurements and IP-GDGT has a larger proportion in the lipid extract. Whether this is due to fluctuations between the instruments, due to growth conditions or statistical fluctuations can not be clearly stated.

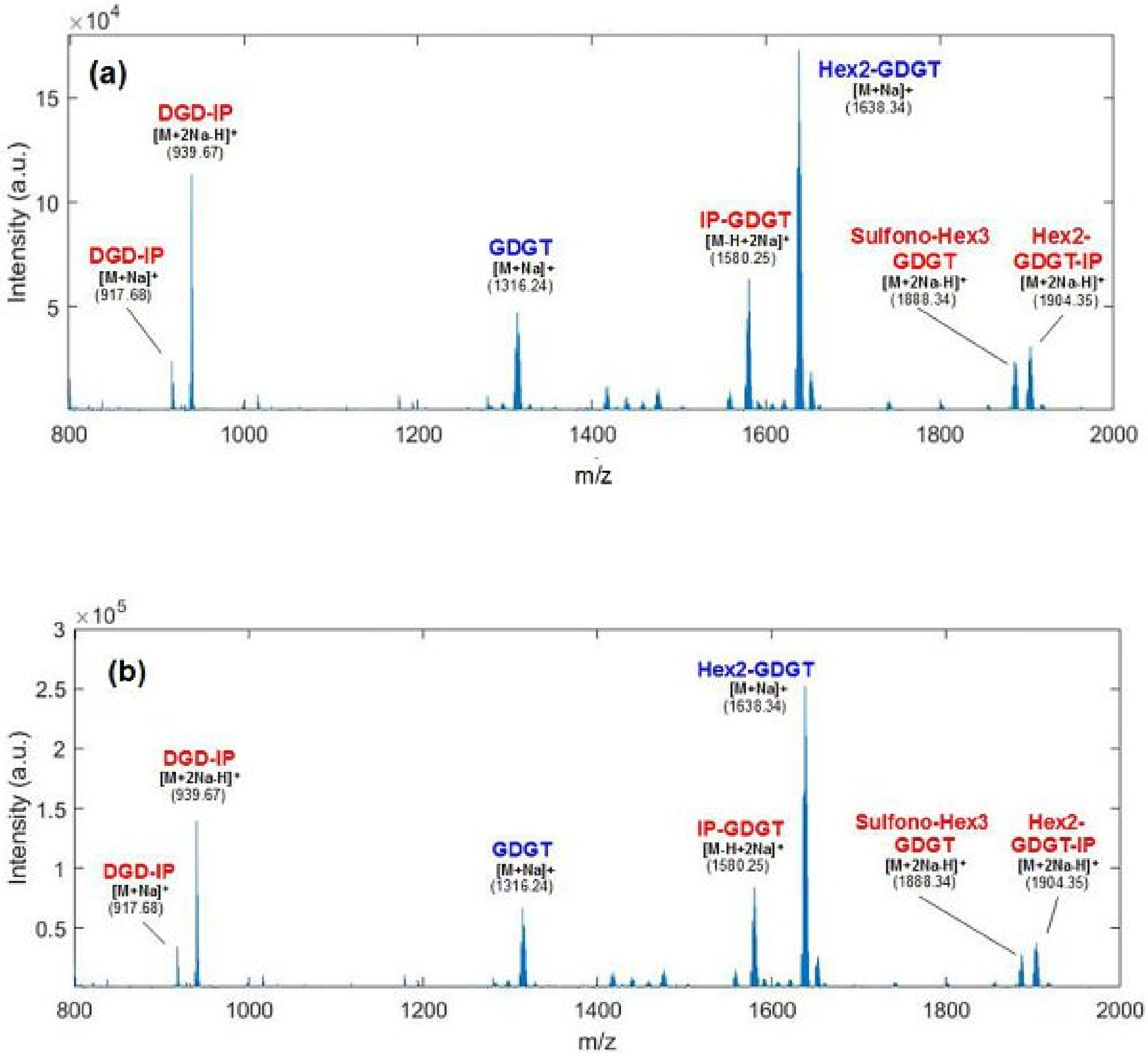

Figure 30: Comparison of sample F3TEL 12 of *S. acidocaldarius* extracted at different points of time during the production process. In (a) bleed 6.1 is shown, (b) shows bleed 13. Both samples were measured on Synapt G2 HDMS in positive ion mode with THAP as a matrix.

In order to get an estimation of biological reproducibility, two samples of the same production process, extracted at different times of the fermentation, were compared to each other. The bleeds 6.1 and 13 originate from the sample F3 TEL 12. Bleed 6.1 was harvested on May 25^{th} 2020 and bleed 13 was harvested on June 16^{th} 2020. The measured spectra, presented in figure 30, show a clear similarity, although some fluctuations cannot be prevented. The ratios of the components show a certain inconsitency, although this can be explained by statistical fluctuations, but the components contained are exactly the same. Nevertheless, it must be considered that the samples of the TEL fermentations were extracted over a longer period of time. *S. acidocaldarius* goes through different growth phases during the fermentation process, one exponential and one stationary phase [21]. The exact time of sampling is therefore very crucial for the outcome of the measurements which makes it quite difficult to compare these biological samples and allows only a rough estimation of their reproducibility. Nevertheless, the samples seem to correspond well and a certain reproducibility seems to be given.

3.4.6 Comparison of Matrices

The measurements performed on the Synapt G2 HDMS often produced a very weak signal with THAP in negative ion mode, especially for the less abundant components in the spectrum. Potential material loss during TLC separation nevertheless demands a reliable way of reproducibly measuring even the low intensity components had to be found. This was achieved by changing the matrix from THAP to 9-AA for the negative ion mode for samples prepared by TLC separation and extraction from the TLC material. However, a matrix change is also accompanied by a change of the measurement signal. Different components are ionized with a different probability due to different matrices. In order to investigate these differences, sample F3 TEL 12, bleed 13, was measured with both 9-AA and THAP, all other measurement parameters remained unchanged. The laser power was not changed for 9-AA despite the fact that the laser power is not ideal for this matrix. On the one hand, keeping the laser power constant creates a basis of comparison, on the other hand, the lipids to be measured were obtained after TLC extraction and very low abundant, requiring a higher laser power anyway. Therefore a very good signal-to-noise ratio and a high resolution were obtained by keeping the laser power at the default value. It should be noted that 9-AA, as described in literature, can only be used for negative ion mode measurements [22]. Measurements in positive ion mode did not provide a signal.

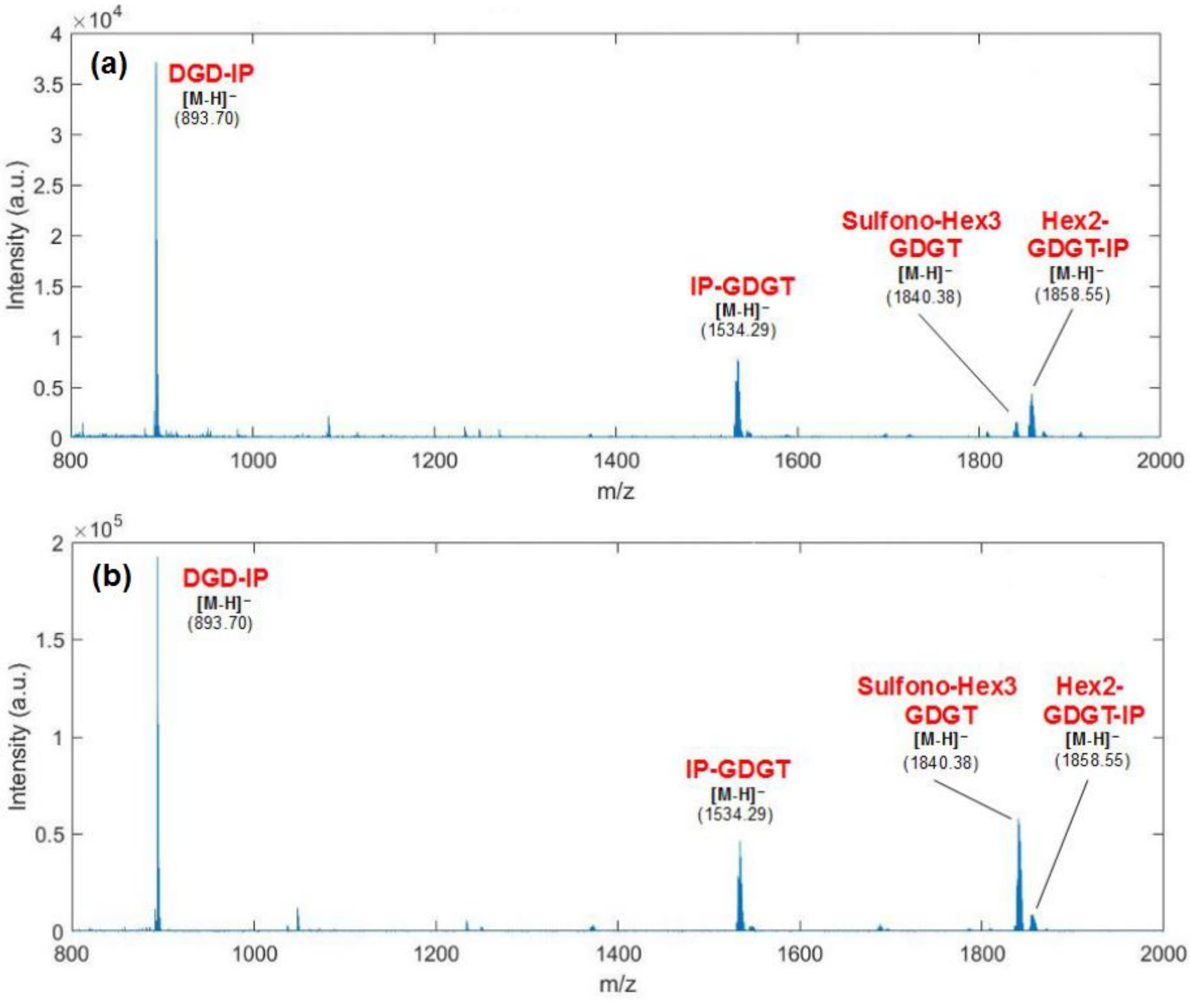

Figure 31: F3 TEL 12, bleed 13 measured in negative ion mode with (a) THAP and (b) 9-AA as a matrix on the Synapt G2 HDMS.

As figure 31 shows, the signal is significantly stronger with matrix 9-AA. The intensity ratios also vary greatly between the two matrices. 9-AA is much more suitable for the measurement of Sulfono-Hex3-GDGT, which is probably due to the preferential ionization in negative ion mode. It increases the measured intensity of Sulfono-Hex3-GDGT quite strongly compared to Hex2-GDGT-IP and all other components, which indicates a very good synergy of the matrix with this component. This behavior is also shown in a measurement on the Shimadzu MALDI-7090, but with a much stronger influence, as shown in figure 32.

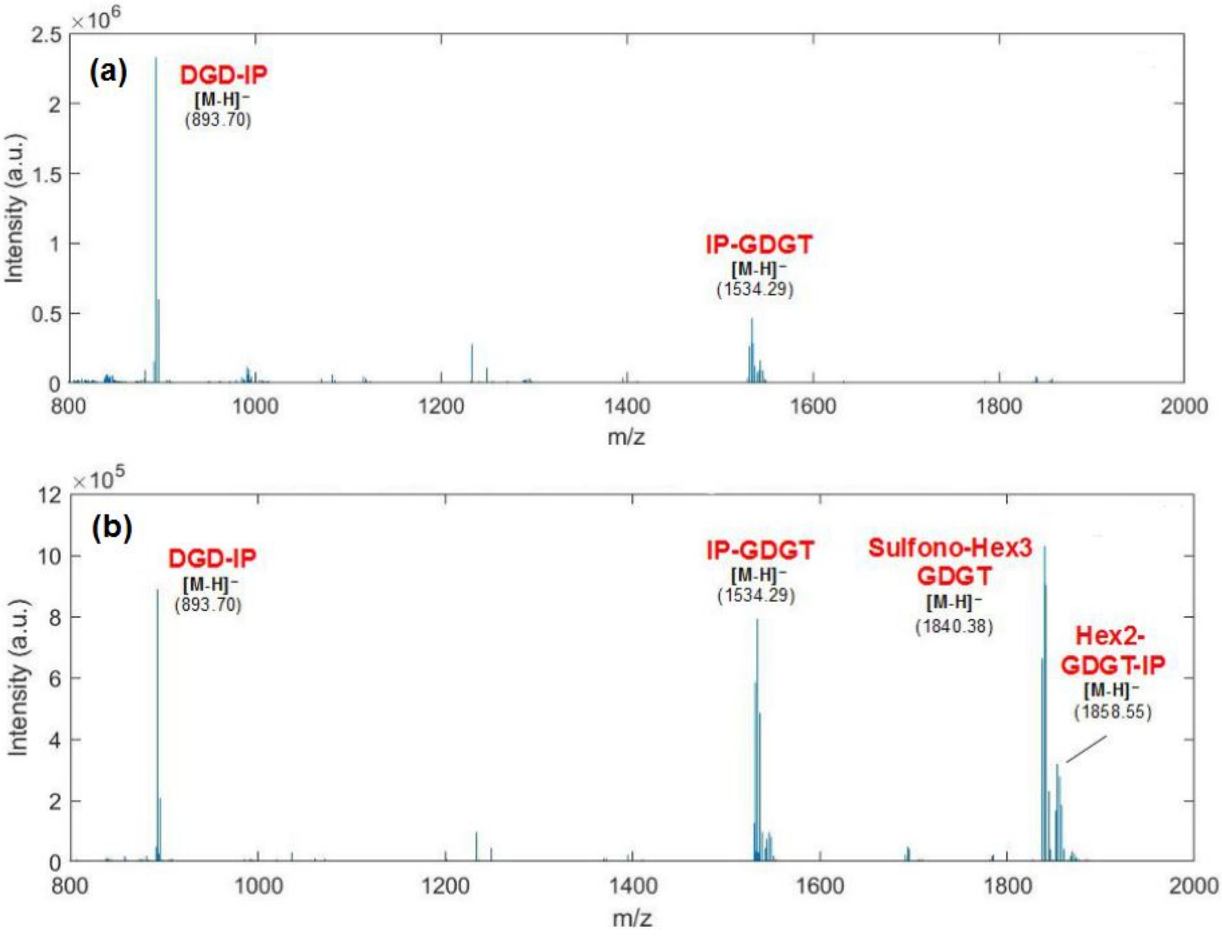

Figure 32: F3 TEL 12, bleed 13 measured in negative ion mode with (a) THAP and (b) 9-AA as a matrix on the Shimadzu MALDI 7090.

A drastic change in the measurement results can be observed. On the one hand, the Shimadzu MALDI 7090 produces a slightly stronger signal for THAP than for 9-AA which can be a random fluctuation. On the other hand, Sulfono-Hex3-GDGT and Hex2-GDGT-IP are measured with very high intensity which cannot be confirmed by any other measurement and can only be observed on the Shimadzu MALDI 7090 with matrix 9-AA. The choice of the matrix seems to have a great influence on the measurement results on the Shimadzu MALDI 7090. Also it has to be kept in mind that the Shimadzu MALDI 7090 has a high vacuum ion source compared to the Synapt G2 which has a intermediate pressure ion source. Measurements on the Synapt G2 HDMS also show a matrix-related variation of the measurement results, but not as significantly. Furthermore Sulfono-Hex3-GDGT and Hex2-GDGT-IP are barely visible in 32a, which might very well be the reason that Sulfono-Hex3-GDGT was not identified in the initial measurements prior to this thesis, as THAP was used for these measurements as well and does almost not show any signal at all for this component.

3.4.7 Comparison of relative intensities of the analytes

One of the biggest disadvantages of MALDI-MS is the inability of quantification of the measured components. After spotting the sample-matrix mixture onto the stainless steel target plate, certain currents occur at the target spot during the evaporation process of the organic solvent resulting in an inhomogeneous distribution of the analyte on the target.

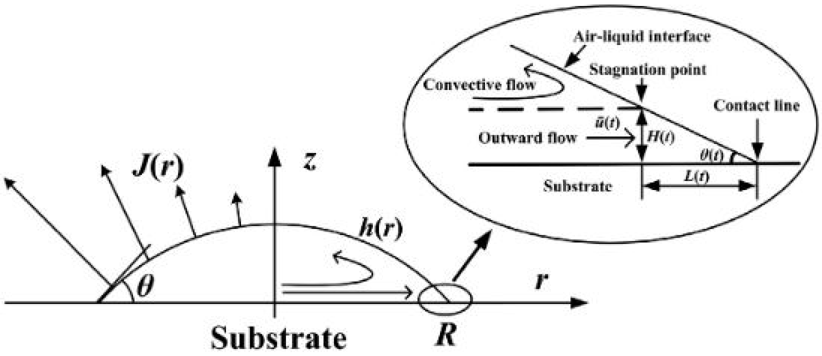

Figure 33: Flowpatterns in an evaporating droplet, adapted from [23].

The evaporation process causes two outward flows, shown in figure 33, an accelerated flow close to the contact line and a constant flow further inside the droplet [23]. This flow also entrains the analyte and deposits it at the edge of the droplet greatly increasing the concentration of the analyte at the edge of the droplet. According to this behavior, the edge of the spot is the location of highest analyte concentration, but the outward flow also leads to inhomogeneities inside the sample spot. Furthermore, the recrystallization process of the matrix-analyte mixture itself leads to an inhomogeneous analyte distribution and the formation of so-called sweet spots which are regions with significantly increased analyte concentrations, and therefore an increased measurement signal. By keeping the parameters constant, an attempt was made to achieve a certain comparability of the measurements.
To estimate the resulting uncertainty, a series of measurements was performed. Under the assumption that the sample-matrix mixture is homogenous, which is very likely as the matrix and analyte are pre-mixed and vor-

texed as liquids in a sample tube, a measurement uncertainty could be calculated. In the first instance, the same sample was applied to 10 spots on the sample plate and the total spot of each target was measured. For this purpose, the laser pathing parameters were changed to a grid and the measurement duration was adjusted so that the entire spot was measured. By ablating the entire spot, the distribution of the components on the target spot is no longer relevant and sweet spots no longer influence the analyte quantification in a negative sense. Differences in the surface texture of the individual spots of the target which could influence the measurement, were neglected.

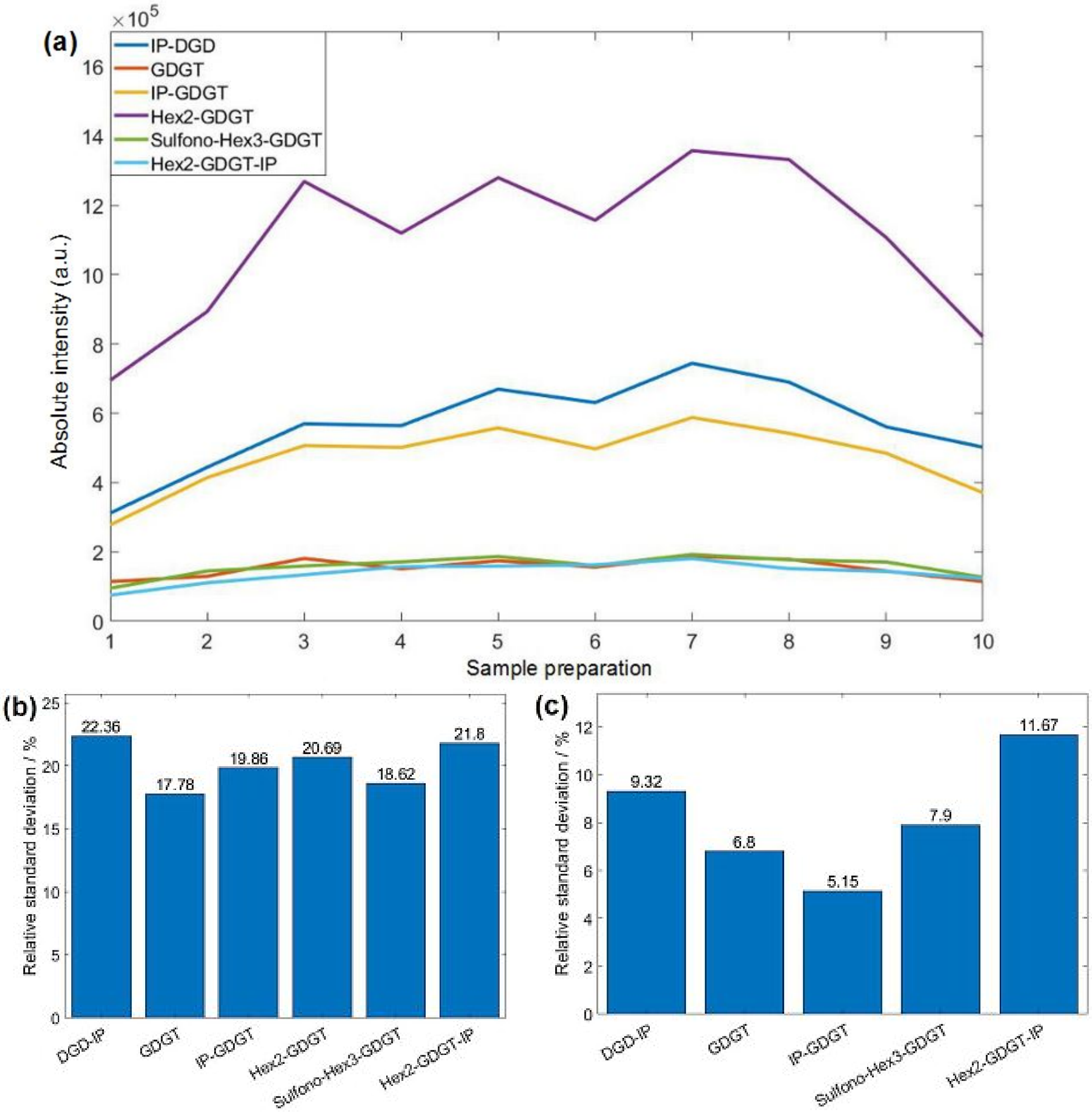

Figure 34: Study of signal fluctuation over ten sample spots.(a) Absolute intensities of six individual components for full ablation of a target spot, (b) standard deviation of the individual components' intensities, (c) standard deviation of signal intensities normalized to Hex2-GDGT.

As Hex2-GDGT was almost always the most abundant component in the lipid extracts measured in this master thesis, it serves as reference to which the relative ratios of the other individual components were calculated. The results of these calculations are shown in figure 34. The signals fluctuate despite keeping the measurement parameters constant. However, one has to keep in mind that the assumption of a homogeneous matrix-analyte mixture is a strong simplification.

The experiment was then repeated under the same conditions and measurement parameters, the only difference being that the measurement time was reduced to 60 seconds and a spiral shape, starting in the middle of the spot, was chosen as laser path. This corresponds to the default measurement procedure of all measurements of this work. Again, Hex2-GDGT serves as reference to which the relative ratios of the other individual components were calculated.

It must be estimated how the outward flow during the evaporation process influences the fluctuations of the ratios of the components to Hex2-GDGT. Although the standard deviation increases compared to the above mentioned experiment, this effect is not so severe as expected, as shown in figure 35. Since all measurements are performed with the same parameters the calculated measurement uncertainty is henceforth assumed for all measurements.

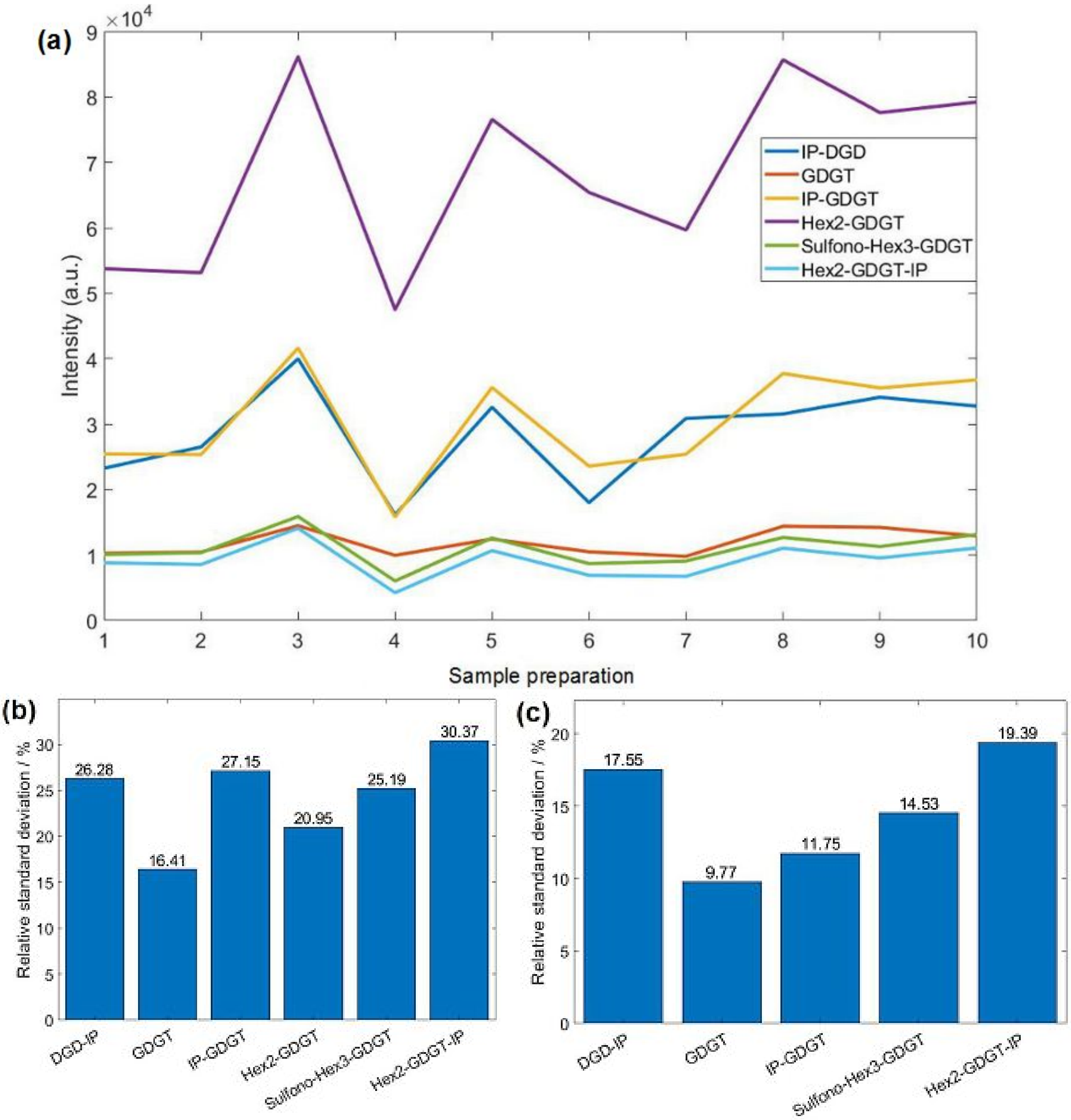

Figure 35: Study of signal fluctuation over ten sample spots.(a) Absolute intensities of six individual components for 60 second ablation, (b) standard deviation of the individual components' intensities, (c) standard deviation of signal intensities normalized to Hex2-GDGT.

3.5 Comparison of Samples

After determining the measurement uncertainties, different samples can be compared to each other and the consequences of changes in the production process can be better estimated. In the course of this work, 11 samples were compared. The samples differed in their production parameters, as described in detail in chapter 2.2.1 .

All comparison studies were based on measurements in the positive ion mode because all measured components could be compared that way. Furthermore, the measurement signal was stronger in the positive than in the negative ion mode, so that statistical fluctuations were not as significant. All measurements were taken according to the Synapt G2 HDMS measurement protocol on the very same instrument a shown in chapter 2.3. The composition of the samples showed a significant variation of the lipid classes in relation to their ratio to each other. It was noticeable that the component Sulfono-Hex3-GDGT was no longer detectable for an increase of the fermentation temperature to T=82°C. However, since an increased temperature was used in only one sample, it could not be confirmed that a causal relationship exists.

The only highly variable parameter between the samples was the biomass concentration and to some extent the dilution rate. However, there seemed to be no causal relation between the percentage of lipid components to the biomass concentration or the dilution rate. Since the fermentation processes were not uniform, there are too many varying parameters to establish a clear causal relationship. The biomass of the TEL fermentations was collected over a longer period of time, while those of the CC fermentations represented a punctual sampling. Furthermore, according to our collaborator, some samples might not yet have reached growth equilibrium in the culture which might have had a major influence on the distribution of lipid components in the extract and distorted the data.

According to [21], there are different growth phases in the lipids of, among others, *S. islandicus*, a close relative to *S. acidocaldarius*. The time of collection influences the composition of the lipid extract. However, there was no data at what point in time of the growth phase at which the lipids were taken. This behavior could not be characterized, but possibly the time of extraction differed between the samples, which is why no correlation could be found between the parameters available and the distribution of the lipids. However, a clear correlation between the biomass concentration and ring numbers could be established, as shown in figure 36. Ring numbers were calculated according to the newly developed calculation algorithm described in chapter 3.2.2.

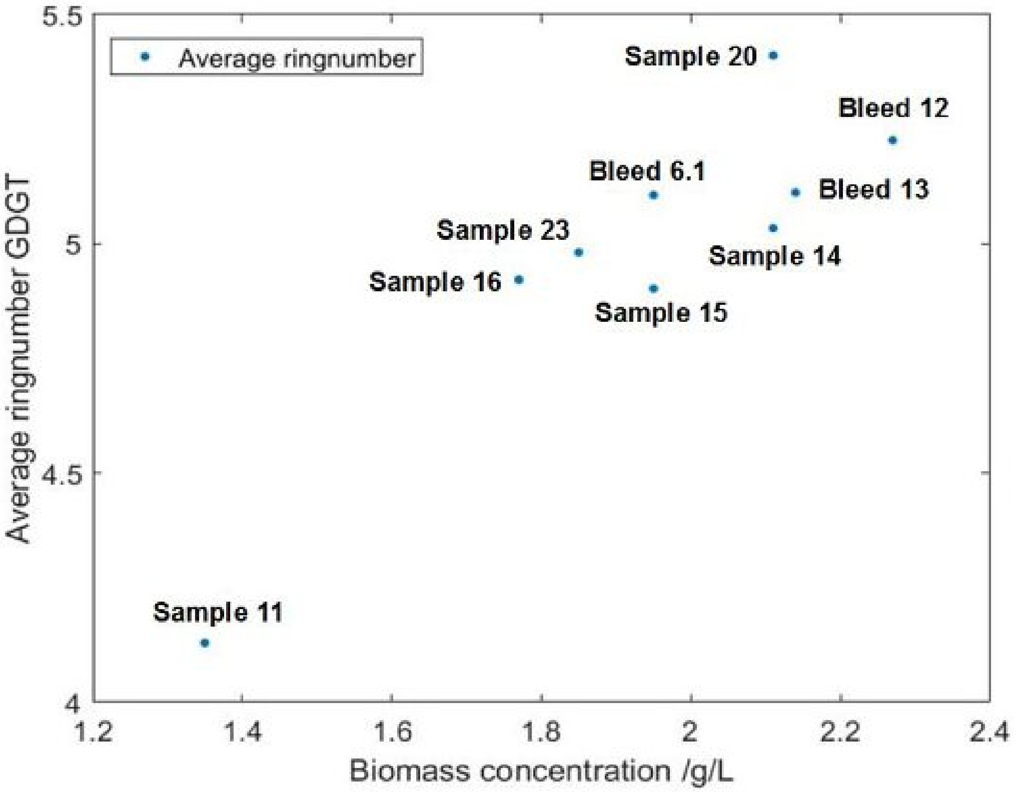

Figure 36: Average ring number of GDGT for different biomass concentrations.

Increasing the biomass concentration leads to an increased number of cyclopentane in the isoprenoid chains. This trend can be seen in all lipid components, the plots are shown in the appendix in section 6.6. Influences of the dilution rate on the number of cyclopentane are not consistent. It can not be estimated whether a change in dilution rate has an influence or not. It must be kept in mind that many parameters influencing cyclopentane formation are unknown and only very strong correlations can be clearly recognized. As shown in the figure 36, there are two samples with the same biomass concentration but different average ring numbers. This behavior can be influenced by many parameters, yet the influence of biomass concentration outweighs these unknowns and seems to be the dominating factor for the number of cyclopentane. As shown in figure 37a, there is a trend showing that increasing the dillution rate reduces the average number of cyclopentane in the lipid components. This behavior has been reported by Quehenberger et al. [3]. Our measurements can not confirm this trend because of all the unknown parameters and variances but the trend can be observed. The dilution rate's influence is much weaker than that of the biomass concentration.

The data point at a dilution rate of 0.3 h^{-1} corresponds to sample 11 which has the lowest biomass concentration by far which strongly overshadows the influence of the dilution rate.

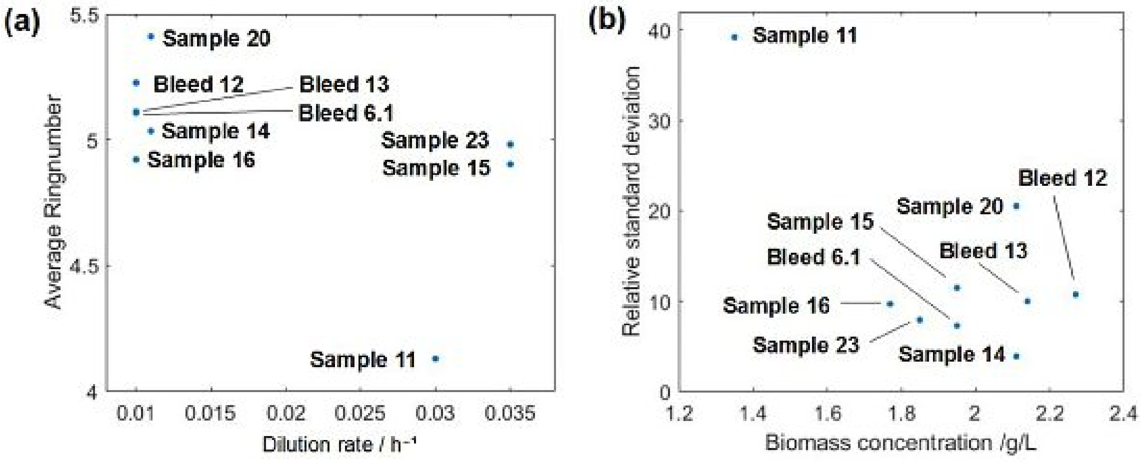

Figure 37: Characterizations for the behavior of GDGT's ring structures. In (a) the average ringnumber depending on the dilution rate is shown, (b) shows the relative standard deviation of the ratio of rings present dependent on the biomass concentration

The standard deviations of the ring numbers show another interesting behavior. At very low biomass concentrations, mainly lipids with 4 cyclopentane, making up more than 75 % in each of the observed lipid components, are formed. The three samples with the lowest biomass concentrations, number 4,9 and 11, show this behavior. However the signal intensity of samples 4 and 9 is really low and is superimposed with an impurity distorting the spectrum. For this reason samples 4 and 9 are not shown in the plots, their data not being reliable. Nevertheless, the trend that mainly lipids with 4 cyclopentane at low biomass concentration are being formed can be recognized in their spectra, making up by far the largest proportion of the lipid cluster. At higher biomass concentrations, the proportions of lipids with different cyclopentane numbers are much more balanced. In figure 37b, the standard deviations of the relative proportions of the rings present are shown. A smaller standard deviation implies a more even distribution of rings among the component, a high standard deviation implies that a specific amount of cyclopentane is dominant in the lipid component, e.g. in sample eleven mainly lipids with four cyclopentane are present.

4 Conclusion

The main aim of this diploma thesis was to establish a reproducible TLC method to be a rapid test for the future production process of our collaborator. This goal was achieved with certain limitations since the separation of the components was only possible via their head groups. Therefore, two blank runs were performed in $CHCl_3$:MeOH (1:1,v/v) on 4 TLC plates (22 mm x 80 mm). Afterwards the plates were activated at 180 °C for five minutes. Subsequently, 6 spots a 5 µl of lipid sample were spotted onto each plate. The TLC plates were developed in LM and then dried. To visualize the lipids, the plates were sprayed with a 0.05% primuline solution.Under UV light of wavelength 365 nm, the bands were scraped off and the silica gel of the same bands were pooled into a safelock tube. To the scraped TLC material, 60 µl of $CHCl_3$:MeOH (2:1,v/v) was added and the mixture was placed in an ultrasonic bath for 15 minutes. After brief centrifugation, the supernatant is drawn off and mixed with the matrix used in a 1:1 ratio and can then be measured. The method developed is technically reproducible. Instrument-specific quantification parameters were calculated allowing an estimation of the measurement uncertainties and the systematic error of in source fragmentation in our measurements. This allows comparisons between different measurements.

A further aim was to identify all lipids in the lipid extract of *S. acidocaldarius* which was confirmed by fragmentation experiments. The isotope distribution of the TELs - seeming uncommon at first sight - turned out to be a superposition of the same lipids with a different number of cyclopentane rings in their core structures. In order to calculate the cyclopentane ring distribution of the lipids, an algorithm was designed in Matlab. Based on its results, an analysis of different samples was performed with respect to their lipid component distributions and the cyclopentane ring distributions of the individual lipid components. No causal relationship between the parameters available to the distribution of the components could be found, as there are many unknown variables influencing the fermentation process to an unknown extent. This is hardly surprising but a clear causal relationship between the biomass concentration and the cyclopentane ring distribution in all lipid components could be found.

Furthermore, the biological reproducibility of the fermentation process was investigated. The reproducibility seems to be given according to the data but it is difficult to confirm due to those unknown parameters. It was finally investigated if samples dissolved in DMSO/isopropanol facilitating the liposome formation process, differ from samples dissolved in $CHCl_3$/MeOH. Since the measurement indicates that this has no significant effect on the composition of the sample, dissolving the extract in DMSO/isopropanol seems to be possible without any problems.

5 Acknowledgments

At this point, I would like to thank my supervisors Univ. Prof. Mag. Dr. Martina Marchetti-Deschmann and Ao. Univ. Prof. Mag. Dr. Ernst Pittenauer for the intensive supervision, the support and the helpful suggestions throughout the last year. Since my backgorund is not in analytical chemistry, I particularly appreciate your dedication and patience.

I would also like to thank my colleagues who supported me so kindly, especially at the beginning of my thesis, and taught me so much about the working methods in analytical chemistry, which helped me a lot, since I did not have very much experience working in a lab. Especially Stephi, Sam and Stefan, I would like to thank you for your patience and valuable input. I hope I can return the favor to you in the years to come.

Also, a big thank you to my girlfriend Nina, who has always supported me over the last year and put up with me even in the most stressful stages of this thesis.

I would also like to thank my parents very much, who have made my education possible in the first place and have always supported me unconditionally in every phase of this thesis and throughout my studies. Special thanks also once again to my Mom, who has helped me to improve this thesis grammatically and linguistically sometimes until well after midnight. Especially to you I would like to dedicate this work.

I would also like to thank Dr. Julian Quehenberger for his helpful information and suggestions on the samples I received, for which he always immediately took time.

Last but not least I want to thank my whole family and especially both of my sisters, who are always there for me and always have been as my very best friends.

Thank you all for the support in these challenging times, without you I would not be at the point in my life where I am now.

6 Appendix

6.1 Structures of *S. acidocaldarius* membrane lipids

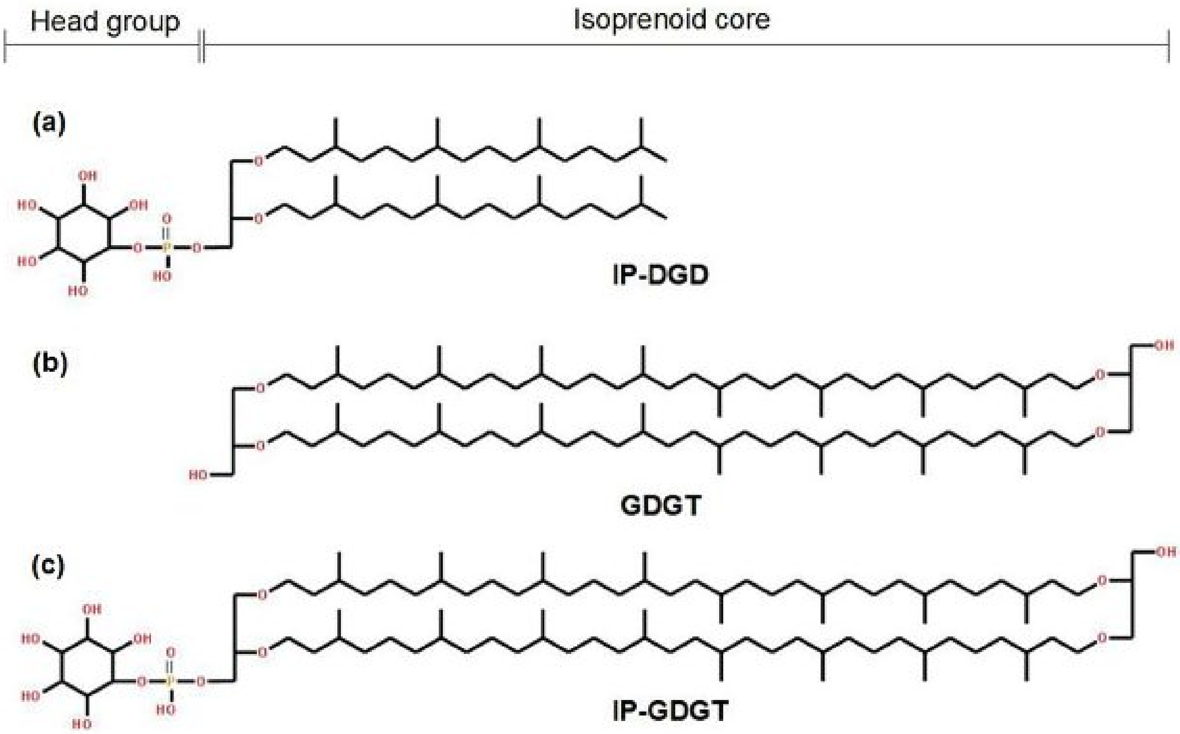

Figure 38: Preliminary structures of (a) IP-DGD, (b) GDGT and (c) IP-GDGT

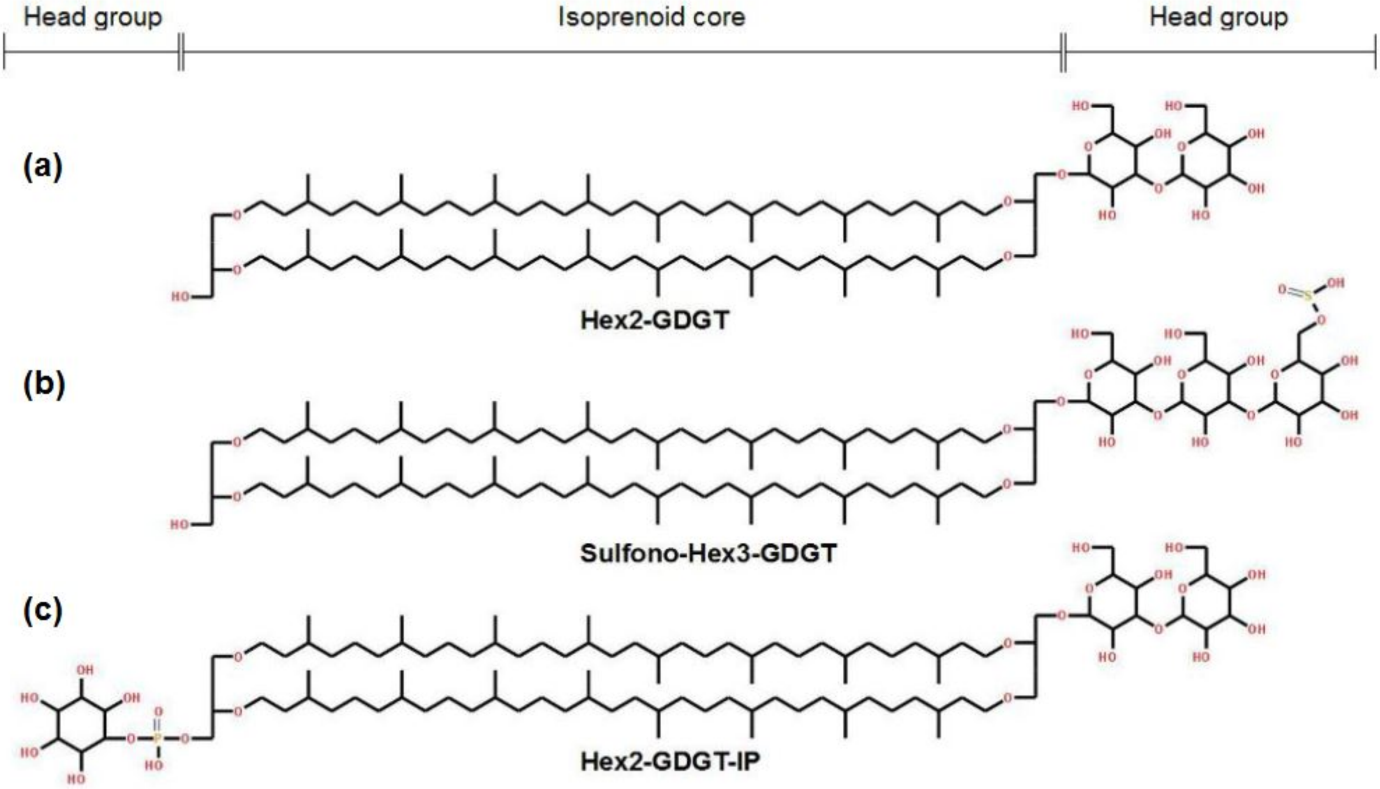

Figure 39: Preliminary structures of (a) Hex2-GDGT, (b) Sulfono-Hex3-GDGT and (c) Hex2-GDGT-IP

6.2 TLC Mobile and Stationary Phases

Stationary Phase	Mobile Phase	(v/v)	Separation
RP-18	MeOH : MTBE	(5.95:1.05)	No separation
RP-18	MeOH : MTBE	(5.25:1.75)	No separation
RP-18	MeOH : MTBE	(4.9:2.1)	No separation
RP-18	MeOH : MTBE	(4.55:2.45)	No separation
RP-18	MeOH : MTBE	(3.85:3.15)	No separation
RP-18	MeOH : MTBE : H_2O	(6.3:0.7:0.27)	No separation
RP-18	MeOH : MTBE : H_2O	(6.65:0.35:0.27)	No separation
RP-18	MeOH : MTBE : H_2O	(6.44:0.56:0.27)	No separation
RP-18	$CHCl_3$: MeOH : H_2O	(5:0.5:0.5)	No separation
RP-18	$CHCl_3$: MeOH : H_2O	(4.5:1:0.5)	No separation
RP-18	MeOH : MTBE : H_2O : HCOOH	(4.5:0.5:0.25:0.05)	No separation
RP-18	MeOH : MTBE : n-Heptan	(3:1.5:0.5)	No separation
RP-18	MeOH : MTBE : n-Heptan	(3:1.75:0.25)	No separation
RP-18	MeOH : MTBE : n-Heptan	(2.5:2.25:0.25)	No separation
RP-18	n-Heptan : MeOH	(5:1)	No separation
Silica Gel 60 A	$CHCl_3$: MeOH : 0.1M H_2SO_4	(60:10:1)	Separation in 3 spots
Silica Gel 60 A	$CHCl_3$: MeOH : 0.1M H_2SO_4	(55:15:1)	Separation in 3 spots
Silica Gel 60 A	$CHCl_3$: MeOH : 0.1M H_2SO_4	(50:20:1)	Separation in 3 spots
Silica Gel 60 A	$CHCl_3$: MeOH : 0.1M H_2SO_4	(48:22:1)	Separation in 3 spots
Silica Gel 60 A	$CHCl_3$: MeOH : 90% acetic acid	(65:4:35)	Separation in 3 spots

6.3 Background Contaminants

Table 6: Positive Ion Mode

Monoisotopic Ion Mass	Possible Origin
812.5	TLC compound
837.0	Matrix compound of THAP
875.4	TLC compound
907.5	TLC compound
997.61	Matrix compound of THAP
1012.4	TLC compound
1015.7	Matrix compound of THAP
1031.7	Matrix compound of THAP
1177.8	Matrix compound of THAP
1199.7	Matrix compound of THAP
1208.3	Matrix compound of THAP
1257.7	TLC compound
1215.7	TLC compound
1329.9	Matrix compound of THAP

Table 7: Negative Ion Mode

Monoisotopic Ion Mass	Possible Origin
813.1	Matrix Compound of THAP
1047.7	Matrix Compound of 9-AA
1083.7	Matrix Compound of THAP
1233.5	Matrix Compound of 9-AA
1249.8	Matrix Compound of 9-AA
1271.7	Matrix Compound of THAP
896.0	TLC Compound
927.0	TLC Compound
957.0	TLC Compound
1193.0	TLC Compound

6.4 Technical Reproducibility Measurement Spectra

6.4.1 Band 1, positive ion mode

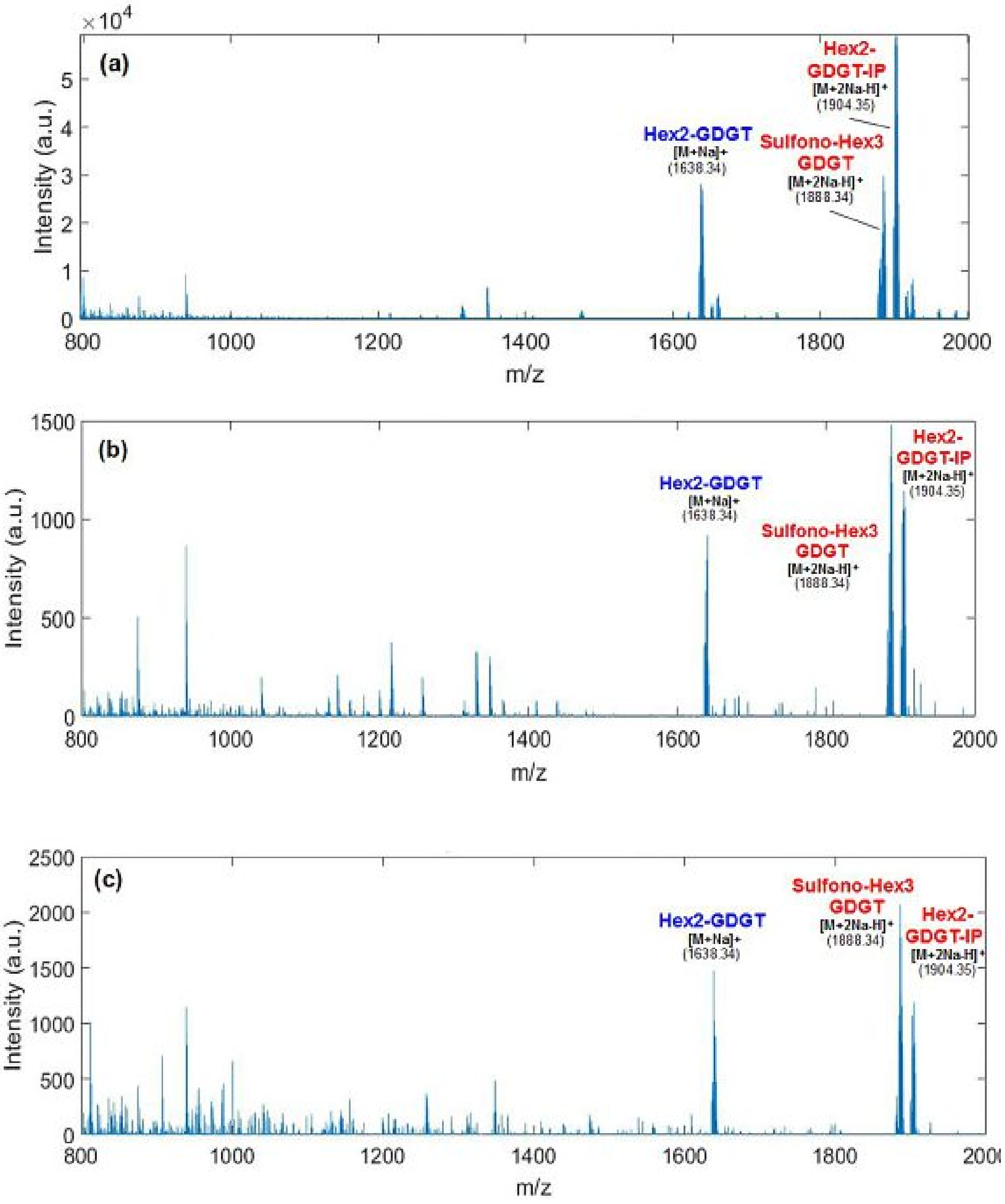

Figure 40: Measurement of lipids extracted from band 1 in positive ion mode, measured on the Synapt G2 HDMS with THAP as matrix. Each of the three TLC developments and associated measurements was carried out on a different day under the same conditions.

6.4.2 Band 2, positive ion mode

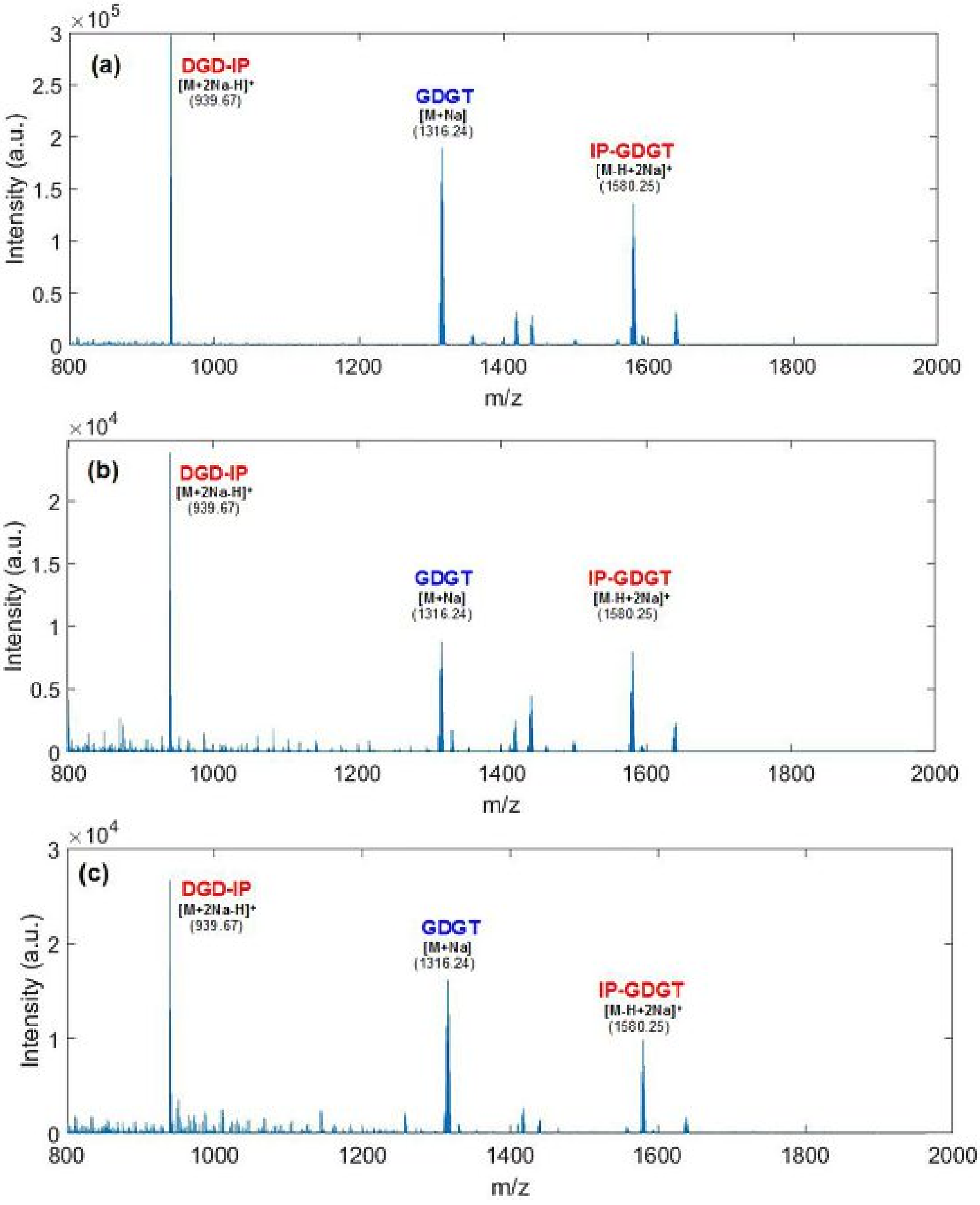

Figure 41: Measurement of lipids extracted from band 2 in positive ion mode, measured on the Synapt G2 HDMS with THAP as matrix. Each of the three TLC developments and associated measurements was carried out on a different day under the same conditions.

6.4.3 Band 3, positive ion mode

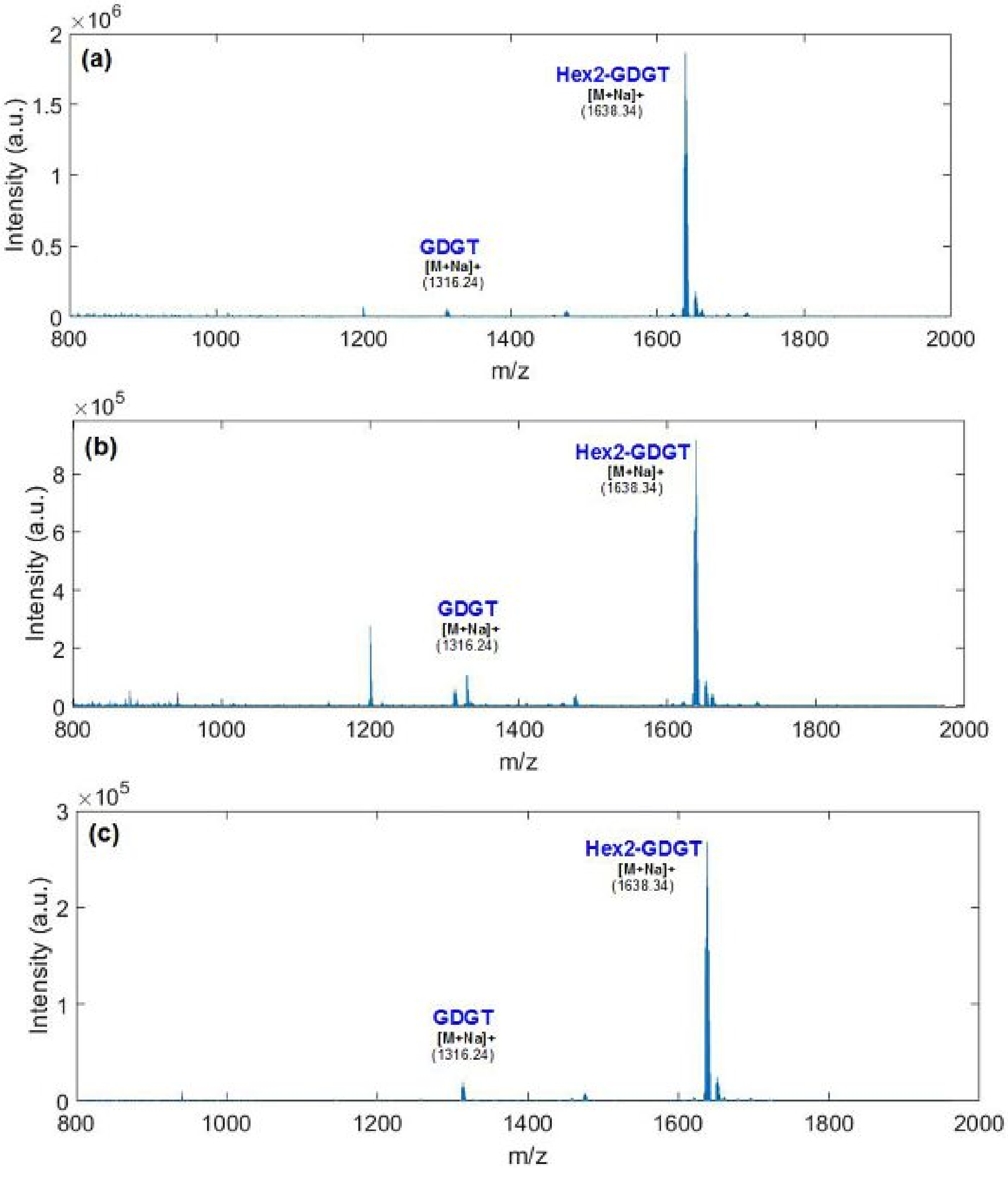

Figure 42: Measurement of lipids extracted from band 3 in positive ion mode, measured on the Synapt G2 HDMS with THAP as matrix. Each of the three TLC developments and associated measurements was carried out on a different day under the same conditions.

6.4.4 Band 1, negative ion mode

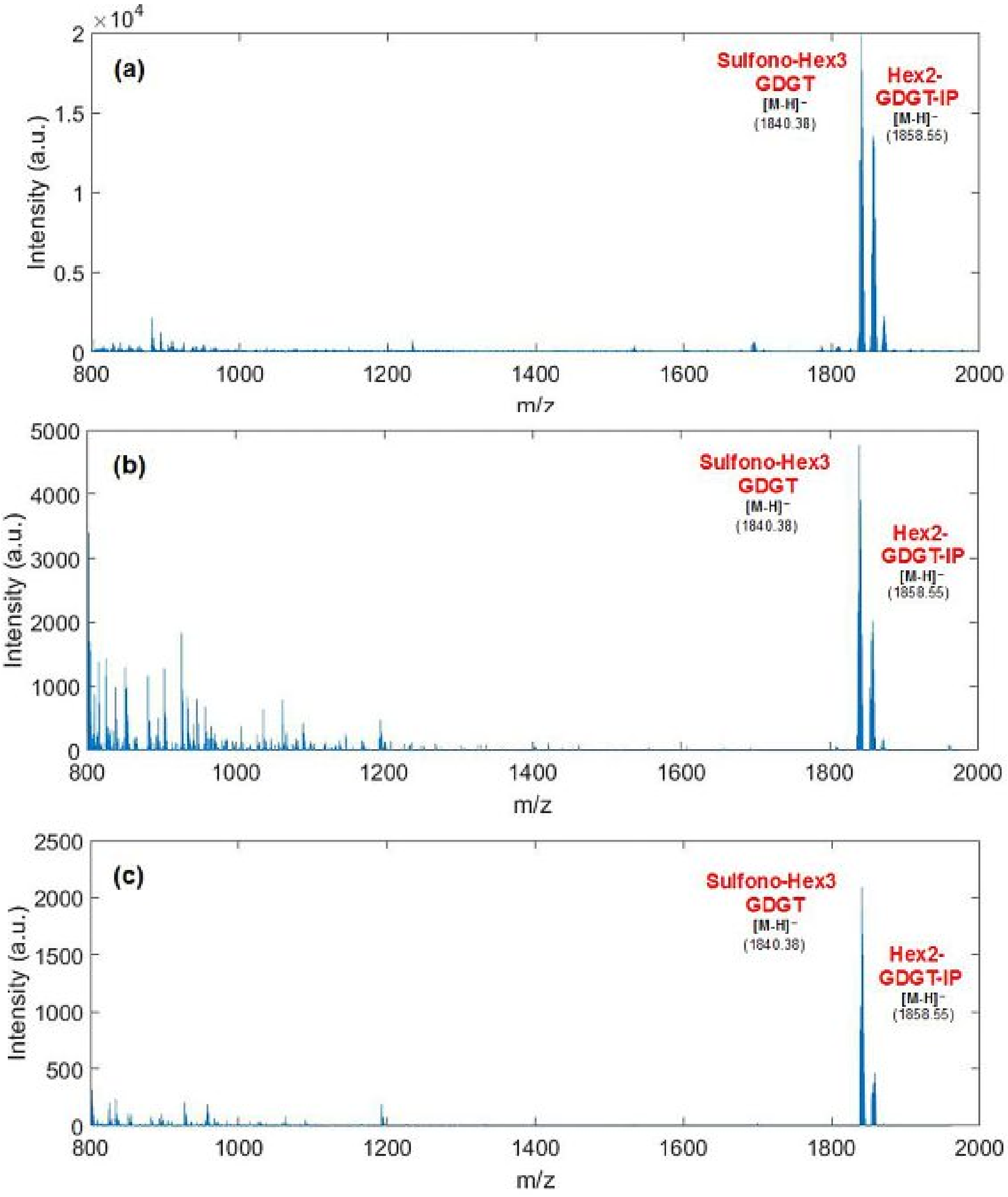

Figure 43: Measurement of lipids extracted from band 1 in negative ion mode, measured on the Synapt G2 HDMS with 9-AA as matrix. Each of the three TLC developments and associated measurements was carried out on a different day under the same conditions.

6.5 Ringdistribution Algorithm

The algorithm to characterize the ringdistibutions of *S. acidocaldarius* was developed in MATLAB R2019b, but can be used in newer MATLAB versions as well if minor adaptations are performed.

```
function [x,avg,err] = Ring_distribution(iso,peaks_meas,rings,Spec,r0)
%%
% Input:       iso = isotope distribution, must be the same
%                    length as the  array for the
%                    measured peaks
%       peaks_meas = 2-dimensional array, column 1 conatining
%                    the m/z conatining the m/z  ratio,
%                    column 2 the intensity of the respective
%                    peak. The array has to contain an even
%                    number of lines (4x2,6x2, 8x2 ...)
%            rings = Maximum amount of rings expected, integer
%            Spect = 2-dimensional array of the spectrum
%                    column 1 conatining the m/z ratio,
%                    column 2 the intensity of the signal
%                    measured
%               r0 = if Species with 0 rings is expected
%                    r0=0, else r0=1
%
% Output:           x = array with the distribution of the
%                       rings starting with the highest number
%                       of rings
%                 avg = average ringnumber
%                   plot of distirbution
%
% The function calculates the distribution utilizing the
% 2nd peak, since this is the most intense peak due to the
% isotope distribution in this mass range.
%
%%

R_stack=[];
clear r
clear rel_peaks
```

```
amount=0;
count=0;
x=[];
count1=0;
avg=0;
peaks_meas=peaks_meas';
while rings>length(peaks_meas)/2
    rings=rings-1;
    count=count+1;
end
%% calculation of the ringdistribution

for i=1:rings+1
    r(i,:)=iso;
    iso(end-1:end)=[];
    iso=[0,0,iso];
end

for i=1:rings
%     if rings>length(peaks_meas(2,:)/2)
%         break
%     end
    rel_peaks(i,:)=r(i,:).*peaks_meas(2,i*2)/100;
    peaks_meas(2,:)=peaks_meas(2,:)-rel_peaks(i,:);
end

if r0==0
    rel_peaks(i+1,:)=r(i+1,:).*peaks_meas(2,i*2+2)/100;
        peaks_meas(2,:)=peaks_meas(2,:)-rel_peaks(i+1,:);
end

%% ring distributiion

for i=1:rings
    amount=amount+rel_peaks(i,2*i);
end
if r0==0
    amount=amount+rel_peaks(i+1,2*i+2);
end

for i=1:rings
```

```
    x=[x,rel_peaks(i,2*i)/amount];
end
if r0==0
    x=[x,rel_peaks(i+1,2*i+2)/amount];
end

%% average rings

if r0==0
    for i =1:rings+1
    avg=avg+x(end+1-i)*(i+count-1);
    end

else
for i =1:rings
    avg=avg+x(end+1-i)*(i+count);
end
end

%% plot
for i=1:rings
    R_stack=[R_stack;rel_peaks(i,:)];
end
if r0==0
    R_stack=[R_stack;rel_peaks(i+1,:)];
end
contro=max(R_stack(end-1,:));
if contro<max(max(R_stack))*0.05
    R_stack(end-1:end,:)=[];

end
contro=max(R_stack(end,:));
if contro<max(max(R_stack))*0.05
    disp('care stack')
    R_stack(end,:)=[];
end

if count>0
    rings=rings+count;
end
figure()
```

```
bar(peaks_meas(1,:),R_stack','stacked','barwidth', 0.5)
if rings==7
legend('7 rings','6 rings','5 rings','4 rings','3 rings','2 rings','1 ring','0 rings')
elseif rings==6
    legend('6 rings','5 rings','4 rings','3 rings','2 rings','1 ring','0 rings')
elseif rings == 5
    legend('5 rings','4 rings','3 rings','2 rings','1 ring','0 rings')
elseif rings == 4
    legend('4 rings','3 rings','2 rings','1 ring','0 rings')
elseif rings == 3
    legend('3 rings','2 rings','1 ring','0 rings')
elseif rings == 2
    legend('2 rings','1 ring','0 rings')
else
    disp('Error ring structures.')
end
hold on
plot(Spec(:,1),Spec(:,2),'k','Linewidth',2,'DisplayName','Spectrum')
hold off
xlabel('m/z')
ylabel('Intensity (a.u.)')

title('Number of Cyclopentane in Lipid')
set(gca,'FontSize',18)

%%

g=0;
h=1;
x=x*100;
while h==1
    h=0;
    g=g+1;
    for i = 1:length(x)
        if x(i)<=0
            x(i)=0;
            h=1;
```

```
        end
    end
    if h==1
        x(end)=[];
    end
end
g=g-1;
tro=length(x)
for i=1:length(x)
    if length(x)<tro

        x(end)=[];
        count1=count1+1;
        break
    elseif x(i)<2
        x(i)=[];
        disp('extra')
        count1=count1+1;
    end
end

x=round(x,2)
figure()
f=flip([rings-length(x)+1:rings]);
bar(f,x);
if r0==0
    text(flip(1:length(x))+count+g-1,x,num2str(x'),'vert','
       bottom','horiz','center','FontSize',15);
else
    text(flip(1:length(x))+count+g+count1,x,num2str(x'),'vert',
       'bottom','horiz','center','FontSize',15);
end
box off
xlabel('Number of rings')
ylabel('relative intensity / %')
legend('Number of rings','Location','northwest')
title(['Distribution of rings, average ringnumber = ',num2str(
   avg),' rings.'])
set(gca,'FontSize',15)
ylim([0 max(x)*1.2])
x=x';
```

```

err=[peaks_meas(2,1),peaks_meas(2,3),peaks_meas(2,5),peaks_meas(2,7)]
end
```

6.6 Average ring numbers

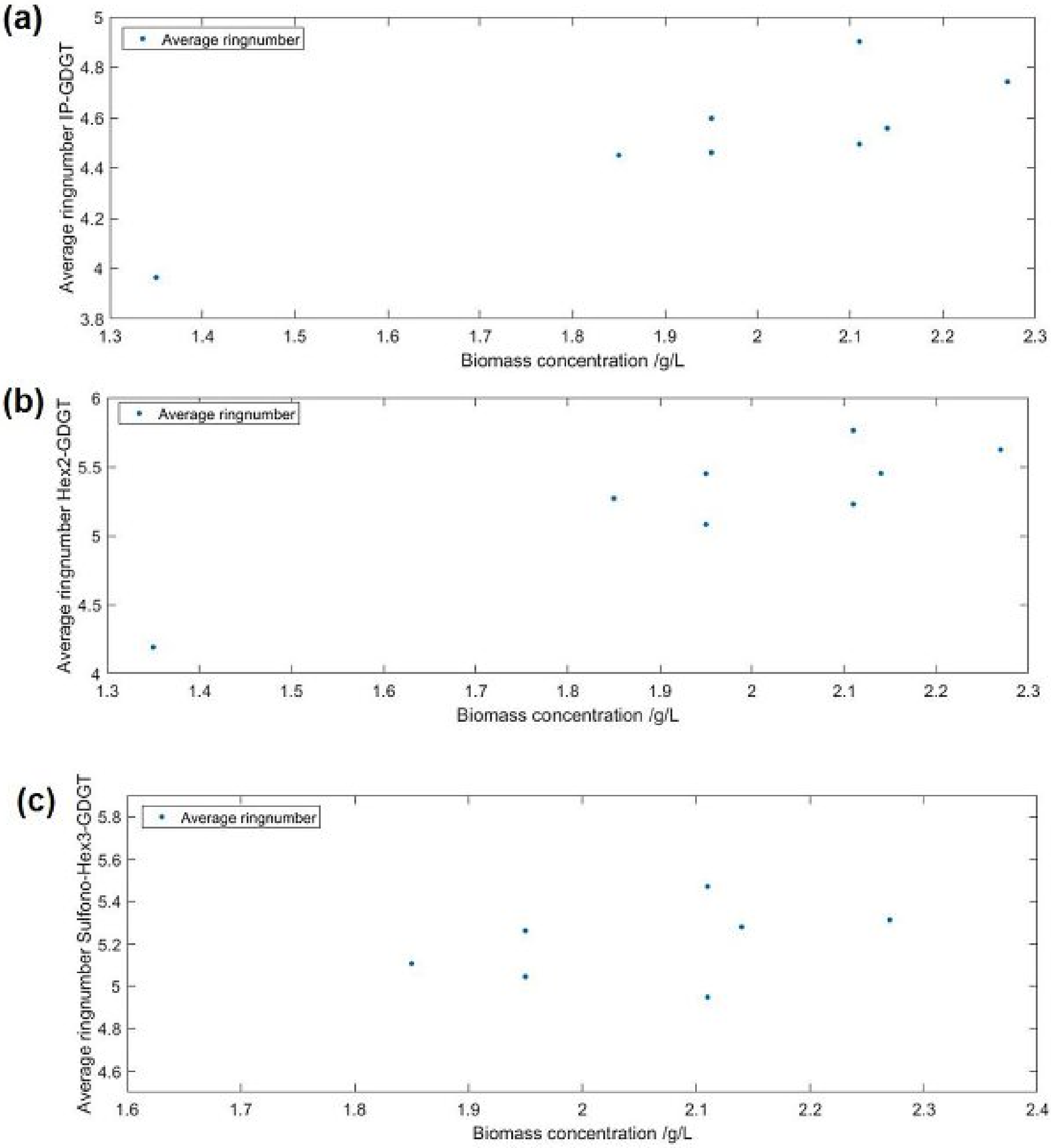

(a) Average ring distribution of Sulfono-Hex3-GDGT.

Figure 44: Average ring distributions of (a) IP-GDGT, (b) Hex2-GDGT and (c) Sulfono-Hex3-GDGT.

References

[1] T. D. Brock, K. M. Brock, R. T. Belly, and R. L. Weiss, "Sulfolobus: a new genus of sulfur-oxidizing bacteria living at low ph and high temperature," *Archiv für Mikrobiologie*, vol. 84, no. 1, pp. 54–68, 1972. Springer.

[2] J. L. Van De Vossenberg, A. J. Driessen, and W. N. Konings, "The essence of being extremophilic: the role of the unique archaeal membrane lipids," *Extremophiles*, vol. 2, no. 3, pp. 163–170, 1998. Springer.

[3] J. Quehenberger, E. Pittenauer, G. Allmaier, and O. Spadiut, "The influence of the specific growth rate on the lipid composition of sulfolobus acidocaldarius," *Extremophiles*, pp. 1–8, 2020. Springer.

[4] S. M. Jensen, V. L. Neesgaard, S. L. N. Skjoldbjerg, M. Brandl, C. S. Ejsing, and A. H. Treusch, "The effects of temperature and growth phase on the lipidomes of sulfolobus islandicus and sulfolobus tokodaii," *Life*, vol. 5, no. 3, pp. 1539–1566, 2015. Multidisciplinary Digital Publishing Institute.

[5] E. Hahn-Deinstrop, "Applied thin-layer chromatography. by elke hahn-deinstrop," 2007. 2007 WILEY-VCH Verlag GmbH & Co. KGaA, Weinheim.

[6] E. Hoffmann, J. J. Charette, V. Stroobant, and J. Trottier, "Instrumentelle analytik und bioanalytik," 2015. Wiley Online Library.

[7] E. Hoffmann, J. J. Charette, V. Stroobant, and J. Trottier, "Mass spectrometry: Principles and applications," 1997. The Atrium, Southern gate, Chichester, West Sussex PO19 8SQ, England: John Wiley & Sons Ltd.

[8] S. Zoratto, "Profiling and imaging of fungal metabolites by MALDI ion mobility MS," 2014. Diploma Thesis, TU Vienna.

[9] M. Karas and F. Hillenkamp, "Laser desorption ionization of proteins with molecular masses exceeding 10,000 daltons," *Analytical chemistry*, vol. 60, no. 20, pp. 2299–2301, 1988.

[10] Wikipedia, "Maldi," 2013. https://commons.wikimedia.org/wiki/File:Maldi.svg, accesed on 2020-12-16.

[11] J. H. Gross, "Massenspektrometrie," 2019. Springer.

[12] D. R. Paschotta, “Micro channel plate,” https://www.rp-photonics.com/microchannel_plates.html, accesed on 2020-12-16.

[13] Waters, “Waters synapt g2 high gefinition mss spectrometry system operator’s overview and maintenance guide, revision a,” 2009.

[14] O. Belgacem, E. Pittenauer, M. Openshaw, P. Hart, A. Bowdler, and G. Allmaier, “Axial spatial distribution focusing: improving maldi-tof/rtof mass spectrometric performance for high-energy collision-induced dissociation of biomolecules,” *Rapid Communications in Mass Spectrometry*, vol. 30, no. 3, pp. 343–351, 2016. Wiley Online Library.

[15] Shimadzu, “Maldi 7090 customer presentation,” 2014.

[16] T. White, S. Bursten, D. Federighi, R. A. Lewis, and E. Nudelman, “High-resolution separation and quantification of neutral lipid and phospholipid species in mammalian cells and sera by multi-one-dimensional thin-layer chromatography,” *Analytical biochemistry*, vol. 258, no. 1, pp. 109–117, 1998. Elsevier.

[17] K. Sládková, J. Houška, and J. Havel, “Laser desorption ionization of red phosphorus clusters and their use for mass calibration in time-of-flight mass spectrometry,” *Rapid Communications in Mass Spectrometry: An International Journal Devoted to the Rapid Dissemination of Up-to-the-Minute Research in Mass Spectrometry*, vol. 23, no. 19, pp. 3114–3118, 2009.

[18] S. M. Jensen, M. Brandl, A. H. Treusch, and C. S. Ejsing, “Structural characterization of ether lipids from the archaeon sulfolobus islandicus by high-resolution shotgun lipidomics,” *Journal of Mass Spectrometry*, vol. 50, no. 3, pp. 476–487, 2015. Wiley Online Library.

[19] R. Angelini, P. Corral, P. Lopalco, A. Ventosa, and A. Corcelli, “Novel ether lipid cardiolipins in archaeal membranes of extreme haloalkaliphiles,” *Biochimica et Biophysica Acta (BBA) - Biomembranes*, vol. 1818, no. 5, pp. 1365 – 1373, 2012.

[20] R. Angelini, F. Babudri, S. Lobasso, and A. Corcelli, “Maldi-tof/ms analysis of archaebacterial lipids in lyophilized membranes dry-mixed with 9-aminoacridine,” *Journal of lipid research*, vol. 51, no. 9, pp. 2818–2825, 2010. ASBMB.

[21] S. M. Jensen, V. L. Neesgaard, S. L. N. Skjoldbjerg, M. Brandl, C. S. Ejsing, and A. H. Treusch, “The effects of temperature and growth phase

on the lipidomes of sulfolobus islandicus and sulfolobus tokodaii," *Life*, vol. 5, no. 3, pp. 1539–1566, 2015. Multidisciplinary Digital Publishing Institute.

[22] R. L. Vermillion-Salsbury and D. M. Hercules, "9-aminoacridine as a matrix for negative mode matrix-assisted laser desorption/ionization," *Rapid communications in mass spectrometry*, vol. 16, no. 16, pp. 1575–1581, 2002.

[23] D. Huang, L. Ma, and X. Xu, "The capillary outward flow inside pinned drying droplets," *International Journal of Heat and Mass Transfer*, vol. 83, pp. 307 – 310, 2015.